Measurement 224 (2024) 113951

Contents lists available at ScienceDirect

Measurement

journal homepage: www.elsevier.com/locate/measurement

# Output-only structural damage identification based on Q-learning hybrid evolutionary algorithm and response reconstruction technique

Guangcai Zhang [a], Jianfei Kang [b], Chunfeng Wan [a,*], Liyu Xie [c], Songtao Xue [c,d,*]

[a] Key Laboratory of Concrete and Prestressed Concrete Structure of Ministry of Education, Southeast University, Nanjing, China
[b] Graduate School of Engineering, Tohoku University, Sendai 980-8572, Japan
[c] Research Institute of Structural Engineering and Disaster Reduction, College of Civil Engineering, Tongji University, Shanghai, China
[d] Department of Architecture, Tohoku Institute of Technology, Sendai, Japan

ARTICLE INFO

*Keywords:*
Damage identification
Evolutionary algorithm
Response reconstruction
Output-only method
Pool strategy
Q-learning algorithm

ABSTRACT

Various structural damage identification methods have been developed and employed, while the absence of input excitation measurements may pose a huge challenge in their application since the input forces such as seismic load, traffic load, wind load, are not directly measurable. To address this issue, in the present paper, a novel output-only structural damage detection approach based on Q-learning hybrid evolutionary algorithm (QHEA) and response reconstruction technique is presented. On the one hand, the external excitation and structural acceleration responses are reconstructed with the aid of response reconstruction and Tikhonov regularization techniques in time domain. Structural damage identification can be formulated as an optimization-based inverse problem. On the other hand, a new optimization framework QHEA integrating Jaya algorithm, differential evolution, Q-learning algorithm is developed as search tool. The unknown structural parameters and unmeasured input force are iteratively updated by using two different measurement sets until the reconstructed acceleration responses agree well with the measured responses. Numerical examples involving a cantilever beam structure under single excitation and a simply-supported 51-bar truss structure under multiple excitations, as well as an experimental five-floor steel frame structure in the laboratory are carried out to validate the effectiveness of the proposed method. The final results demonstrate that the proposed method can accurately detect damage locations and quantify damage extents without the information of input excitation. In addition, the superiority of QHEA over other heuristic algorithms, the uncertainties of measurement noise and modeling errors on damage identification results are further examined.

## 1. Introduction

Major civil infrastructures, such as large-scale bridges, underground pipe gallery, complex spatial structure, high-rise buildings, inevitably accumulate damages during their long-term service life, owing to material deterioration, aging, earthquakes, storms, typhoons, etc. The sudden failure or collapse of the whole structure would lead to enormous casualties and property loss. Therefore, to ensure safe operation of existing engineering structures, it is of significance to perform continuous health monitoring and early damage detection. Over the past two decades, diverse structural damage detection methods have been developed and employed [1,2].

Local non-destructive evaluation methods [3], such as acoustic emission technique, ultrasonic method, thermal field method, have been employed to evaluate the condition of small-scale structures. However, these methods are inappropriate for large-scale and complex structures since they generally require prior knowledge of the location of potential damaged elements. In contrast, vibration-based methods identifying structural damages with global responses, have received more and more attention and they roughly fall into frequency and time domain methods. The first category, frequency domain methods, utilize model properties as damage indicators, frequencies [4], mode shapes [5], modal flexibilities [6], modal strain energy [7], curvature mode shape [8], etc., to identify structural damages. Nevertheless, there are some

* Corresponding authors at: Key Laboratory of concrete and prestressed concrete structure of Ministry of Education, Southeast University, Nanjing, China (C. Wan). Research Institute of Structural Engineering and Disaster Reduction, College of Civil Engineering, Tongji University, Shanghai, China (S. Xue).
*E-mail addresses:* guangcaizhang@seu.edu.cn (G. Zhang), jianfei_kang@foxmail.com (J. Kang), wan@seu.edu.cn (C. Wan), liyuxie@tongji.edu.cn (L. Xie), xue@tongji.edu.cn (S. Xue).

https://doi.org/10.1016/j.measurement.2023.113951
Received 14 October 2023; Received in revised form 22 November 2023; Accepted 27 November 2023
Available online 29 November 2023

inherent disadvantages for most of frequency domain methods. For example, low-order modes are insensitive to small or minor level of elemental damage and high-order modes of a structure are difficult to be precisely obtained despite its more sensitivity. For the latter time domain methods, structural damages are detected by directly using the measured vibration data (accelerations, velocities, displacements, strains, etc.). Raw measurements contain more detailed damage information. Various time domain methods have been developed, such as the least-squares estimation approach [9], the Kalman filter approach [10], the likelihood estimation method [11], the enhanced response sensitivity method [12], the particle filter [13]. In fact, the external excitations, wind load, wave load, vehicle load, etc., acting on the engineering structures are expensive or impossible to be directly acquired, which poses a big challenge to the practical applications.

To solve the issue of absence of excitation measurement, some output-only approaches have been constructed to identify structural damages and input load simultaneously. Chen and Li [14] adopted the modified least-squares approach to iteratively identify unknown structural parameters and input force. Lu and Law [15] employed a damage identification method base on dynamic response sensitivity and gradient-based model updating with output-only measurements. Zhang et al. [16] proposed an effective methodology for simultaneous identification of unknown excitations and damages. Sun and Betti [17] combined the artificial bee colony algorithm and modified Newmark integration scheme. Jayalakshmi and Rao [18] modified Tikhonov regularization technique for force identification and developed an improved version of firefly algorithm for damage identification. Basically, aforementioned methods iteratively update structural parameters and input force at each time step, which would consume considerable computational resources, especially for the complex structures with considerable unknown parameters [19]. Instead of taking the input force time history as unknown parameters, some efforts have been devoted to the approximation of input excitation as a stationary Gaussian white noise [20,21]. For example, Li and Law [22] proposed a new covariance matrix of acceleration responses. Compared with the first few modal quantities, covariance matrix of acceleration presents more sensitive performance to local damages. Lei et al. [23] derived the equation of cross-correlation functions of responses under stationary white noise excitations. Zhang et al. [24] presented a reference-free acceleration correlation functions to locate and quantify the reduction of stiffness and mass parameters. Wang et al. [25] applied the correlation functions between the acceleration responses and strain responses to identify multiple damages. However, it is noted that the assumption of Gaussian white noise process may be invalidate in certain cases. In addition, more than half an hour of recorded signals are required in these researches, which has a negative effect on the computational efficiency.

Compared with correlation function-based methods, the response reconstruction technique does not depend on the type of external excitation, so it is more promising for structural damage detection. Several response reconstruction techniques have been developed in previous studies, such as empirical mode decomposition-based method [26], Kalman filter-based method [27], inverse optimization problem-based method subject to constraints [28], transformation matrix-based method [29]. Among these methods, the dynamical response reconstruction method based on the concept of transmissibility is the most popular, and its basic idea can be simply illustrated [30]. Initially, the measured acceleration responses from the target physical structure are divided into two measurement sets, i.e., set 1 and set 2. Then, the acceleration responses of the measurement set 2 are reconstructed making use of transformation matrix and measurements of set 1. Finally, the unknown parameters of damaged structure are determined by minimizing the discrepancies between the measured accelerations and the reconstructed accelerations. A response reconstruction method was proposed and adopted to detect substructure damage in frequency domain [31], and experimental results of a steel frame structure tests verified its good performance. Subsequently, the wavelet-domain response reconstruction method was developed using unit impulse response function [32]. For the purpose of avoiding data processing, e.g., fast Fourier transform, discrete wavelet transforms, a new response reconstruction in state space domain using Markov system parameters was proposed [33]. Besides, the response reconstruction in time domain for output-only structural damage identification when subjected to seismic loading was also developed [34]. Nevertheless, in these previous researches, model updating methods based on the dynamic response sensitivity was used. It is noted that an appropriate gradient information or a good initial guess of parameters are generally required, which poses a strict requirement on their application for the large-scale structures with limited output-only measurements. Unsatisfactory identification results may be obtained if taking measurement noise and modeling errors into consideration.

Structural damage detection can be mathematically formulated as a constrained optimization-based inverse problem. A proper objective function is defined and optimized by optimization algorithms. Compared with traditional optimization methods, derivative-free heuristic optimization algorithm, such as particle swarm optimization [35], improved whale optimization algorithm [36], modified artificial bee colony algorithm [37], improved butterfly optimization algorithm [38], enhanced bat optimization algorithm [39], grey wolf optimization [40], chaotic bird swarm algorithm [41], have attracted increasing attention owing to their strong search capacity and loose initial conditions [42]. Kim et al. [43] localized and quantified damages of truss structures with differential evolution (DE). Ding et al. [44] developed an improved tree-seed algorithm to identify the hysteretic parameters. A new Jaya algorithm was recently proposed by Rao [45], to address diverse constrained and unconstrained benchmark problems. Different from above-mentioned optimization algorithms, for Jaya algorithm, none of algorithm-specific parameters facilitates the robustness in different applications. Yet, Jaya algorithm has simple mutation mechanism. As an emerging population-based heuristic algorithm, there are deficiencies including weak convergence speed and high possibility of local minima. Shuffling process [46], probability and chaotic searching [47], K-means clustering and a new updating equation [48] have been introduced to improve basic Jaya algorithm. In addition to introducing new improvement mechanisms, hybrid algorithm by combining two or three different algorithms provides another appealing way. Zhang et al. [49] proposed adaptive hybrid Jaya and DE algorithm consisting of Jaya mutation and three mutation strategies of DE. However, the search strategies with Jaya or DE are randomly determined rather than the optimal. In this study, Q-learning hybrid evolutionary algorithm (QHEA) is proposed, and its prominent advantage is that the most suitable search strategy from the strategy pool for each individual can be selected under the guidance of Q-learning.

In this paper, an output-only method making use of QHEA and response reconstruction technique is proposed to identify structural damages with unknown external excitation. Two major contributions are provided. First, response reconstruction technique in time domain is developed to reconstruct external excitation and dynamic responses with the aid of unit impulse response function and Tikhonov regularization. Second, a new optimization framework QHEA including Jaya algorithm, DE and Q-learning algorithm is proposed. Damage locations and severities are detected and qualified by optimizing the objective function established based on the measured and reconstructed acceleration responses using the proposed QHEA. The accuracy, effectiveness, robustness of proposed method is validated with numerical studies on a cantilever beam under single excitation and a 51-bar truss structure under multiple excitations. In addition, a laboratory five-floor steel frame model is used. Furthermore, the uncertainties of measurement noise and modeling error are considered, and the superiority of the proposed QHEA over other heuristic algorithms are investigated.

## 2. Formulations of damage identification

### 2.1. Damage modeling

The structure is discretized into several elements as the finite element method. The structural damages are generally represented by the stiffness reductions. The variation of mass is directly ignored [36,48]. The damage severity of the $i$-th element $\alpha_i$ in the damage modeling is

$$\alpha_i = \frac{E_i - E_i^d}{E_i}, i = 1, 2, ...ne \tag{1}$$

where $E_i$ and $E_i^d$ denote the elasticity modulus of the $i$-th element under the intact and damaged state; $ne$ represents the unknown number of elements. It is noted that $\alpha_i = 0$ indicates a healthy element and $\alpha_i = 1$ implies a totally damaged element.

A series of elemental damage vectors $\alpha = (\alpha_1, \alpha_2, ..., \alpha_i, ...\alpha_{ne})$ within the range of [0, 1] are used to characterize the structural damage model as follows

$$K^d = \sum_{i=1}^{ne} (1 - \alpha_i) K_i^{\text{ele}}, 0 \leqslant \alpha_i \leqslant 1 \tag{2}$$

where $K^d$ and $K_i^{\text{ele}}$ represent the global stiffness matrix in damaged status and the elemental stiffness matrix in healthy status. Structural parameters are equal to $\theta = \{(1 - \alpha_1), (1 - \alpha_2), ..., (1 - \alpha_{ne})\}$.

### 2.2. Response reconstruction method

The equation of motion of a linear multiple degrees of freedom (MDOF) structure subjected to dynamic force can be expressed as

$$M\ddot{u}(t) + C\dot{u}(t) + Ku(t) = Bf(t) \tag{3}$$

where $M$, $C$, $K$ are the mass, damping, stiffness matrices, respectively; $f(t)$ stands for the external excitation; $B$ means the mapping matrix with the value of 1 at the location of input force and 0 at others. Damping matrices can be obtained with Rayleigh damping model as follows

$$C = \beta_1 M + \beta_2 K \tag{4}$$

where $\beta_1$ and $\beta_2$ stand for damping constants.

Structural dynamic responses including displacement vector $u(t)$, velocity vector $\dot{u}(t)$ and acceleration vector $\ddot{u}(t)$ can be acquired with Newmark method.

The acceleration response $\ddot{u}_\mu(t)$ from the $\mu$-th DOF at time $t_n$ can be calculated by

$$\ddot{u}_\mu(t_n) = \int_0^{t_n} \ddot{h}_\mu(t_n - \tau) f(\tau) d\tau \tag{5}$$

where $\ddot{h}_\mu(t)$ indicates the unit impulse response function at the $\mu$-th DOF; $\tau$ stands for the integration variable.

Similar with Eq. (3), the motion equation of linear damped structure subjected to unit impulse excitation can be written as

$$M\ddot{h}(t) + C\dot{h}(t) + Kh(t) = B\delta(t) \tag{6}$$

where $\delta(t)$ stands for the Dirac delta function; $h(t)$, $\dot{h}(t)$, $\ddot{h}(t)$ denote the displacement, velocity, acceleration unit impulse response function, respectively. Unit impulse response functions of structure under the assumption of initially static state could be computed by

$$\begin{cases} M\ddot{h}(t) + C\dot{h}(t) + Kh(t) = 0 \\ h(0) = 0, \dot{h}(0) = M^{-1}B \end{cases} \tag{7}$$

Eq. (5) can be rewritten in discretized form as

$$\ddot{u}_\mu(t_n) = \ddot{h}_\mu(t_n) f(t_n) \tag{8}$$

where $\ddot{h}_\mu(t_n) = \left[\ddot{h}_\mu(t_n), \ddot{h}_\mu(t_{n-1}), ..., \ddot{h}_\mu(t_0)\right]$; $f(t_n) = [f(t_0), f(t_1), ..., f(t_n)]^T$.

For the entire acceleration time history data $\ddot{u}_\mu = \left[\ddot{u}_\mu(t_0), \ddot{u}_\mu(t_1), ..., \ddot{u}_\mu(t_n)\right]^T$, the relationship between output response $\ddot{u}_\mu$ and input force $f$ is

$$\ddot{u}_\mu = H_\mu f \tag{9}$$

where matrix $H_\mu$ is impulse response function matrix, obtained by following equation

$$H_\mu = \begin{bmatrix} \ddot{h}_\mu(t_0) & 0 & 0 & 0 & 0 \\ \ddot{h}_\mu(t_1) & \ddot{h}_\mu(t_0) & 0 & 0 & 0 \\ \ddot{h}_\mu(t_2) & \ddot{h}_\mu(t_1) & \ddot{h}_\mu(t_0) & 0 & 0 \\ \vdots & \vdots & \vdots & \ddots & \vdots \\ \ddot{h}_\mu(t_n) & \ddot{h}_\mu(t_{n-1}) & \ddot{h}_\mu(t_{n-2}) & \cdots & \ddot{h}_\mu(t_0) \end{bmatrix} \tag{10}$$

The response reconstruction methods with unknown input excitation, as described in Refs. [31–34], have been employed and investigated for structural damage identification. Herein, response reconstruction technique in time domain is briefly introduced.

For a target structure, the recorded acceleration responses are initially classified as two measurement sets, namely, measurement set 1 $\ddot{u}_{mea}^{set1}(t)$ and measurement set 2 $\ddot{u}_{mea}^{set2}(t)$, and they can be presented as

$$\begin{cases} \ddot{u}_{mea}^{set1}(t) = H_1 f \\ \ddot{u}_{mea}^{set2}(t) = H_2 f \end{cases} \tag{11}$$

where $H_1$ and $H_2$ denote the matrices associated with unknown structural parameters.

By Eq. (11), the unknown external excitation $f$ and the reconstructed accelerations of measurement set 2 $\ddot{u}_{rec}^{set2}(t)$ are easily acquired when the number of sensors in the measurement set 1 exceeds the number of unknown external excitations

$$f = (H_1)^+ \ddot{u}_{mea}^{set1}(t) \tag{12}$$

$$\ddot{u}_{rec}^{set2}(t) = H_2 (H_1)^+ \ddot{u}_{mea}^{set1}(t) = T_{12} \ddot{u}_{mea}^{set1}(t) \tag{13}$$

where $()^+$ means the pseudo-inverse of a given matrix; $T_{12}$ is the transformation matrix, $T_{12} = H_2 (H_1)^+$.

It is noted that the ill-conditioned nature for force identification problem in Eq. (12) may result in the unstable solution. Hence, to remedy this drawback, an effective method Tikhonov regularization is adopted. The ill-posed inverse problem can be solved as follows

$$f = \left(H_1^T H_1 + \lambda I\right)^{-1} H_1^T \ddot{u}_{mea}^{set1}(t) \tag{14}$$

where $\lambda$ is regularization parameter; $I$ means the identity matrix. Then, the reconstructed accelerations of measurement set 2 $\ddot{u}_{rec}^{set2}(t)$ can be derived as

$$\begin{aligned} \ddot{u}_{rec}^{set2}(t) &= T_{12} \ddot{u}_{mea}^{set1}(t) \\ &= H_2 \left(H_1^T H_1 + \lambda I\right)^{-1} H_1^T \ddot{u}_{mea}^{set1}(t) \end{aligned} \tag{15}$$

A proper regularization parameter $\lambda$ is the key point of Tikhonov regularization technique. In this regard, L-curve method is employed owing to its considerable successful applications. The optimal regularization parameter $\lambda_{op}$ is located at the corner of the L-curve.

In addition, engineering structures may be subjected to multiple external excitations, and this more complex but practical case is further

considered. The dynamic responses of linear structural system under multi-point input force are equal to the superposition of those caused by single excitation. The acceleration response from the $\mu$-th DOF at time $t_n$ can be expressed as

$$\ddot{u}_{\mu}(t_n) = \ddot{u}_{\mu,1}(t_n) + \ddot{u}_{\mu,2}(t_n) + , ..., + \ddot{u}_{\mu,nf}(t_n) = \sum_{i=1}^{nf} \int_0^{t_n} \ddot{h}_{\mu,i}(t_n - \tau) f_i(\tau) d\tau \tag{16}$$

where *nf* means the number of unknown forces.

According to Eq. (5) and Eq. (8), the acceleration response can be given as

$$\ddot{u}_{\mu}(t_n) = \sum_{i=1}^{nf} H_{\mu,i}(t_n) f_i(t_n) \tag{17}$$

where matrix $H_{\mu,i}(t_n)$ is

$$H_{\mu,i} = \begin{bmatrix} \ddot{h}_{\mu,i}(t_0) & 0 & 0 & 0 & 0 \\ \ddot{h}_{\mu,i}(t_1) & \ddot{h}_{\mu,i}(t_0) & 0 & 0 & 0 \\ \ddot{h}_{\mu,i}(t_2) & \ddot{h}_{\mu,i}(t_1) & \ddot{h}_{\mu,i}(t_0) & 0 & 0 \\ \vdots & \vdots & \vdots & \ddots & \vdots \\ \ddot{h}_{\mu,i}(t_n) & \ddot{h}_{\mu,i}(t_{n-1}) & \ddot{h}_{\mu,i}(t_{n-2}) & \cdots & \ddot{h}_{\mu,i}(t_0) \end{bmatrix} \tag{18}$$

Subsequently, response reconstruction method as described in Eqs. (11–15) is adopted to reconstruct the structural responses under multiple unknown forces.

The difference between the measured accelerations $\ddot{u}_{mea}^{set2}(t)$ and reconstructed ones $\ddot{u}_{rec}^{set2}(t)$ of the second measurement set from the damaged structure is set as objective function

$$f_{obj} = \left\| \ddot{u}_{mea}^{set2} - \ddot{u}_{rec}^{set2}(\theta) \right\|_2 \tag{19}$$

where $f_{obj}$ means the objective function; $\theta$ denotes the unknown structural parameters to be identified. The unknown structural parameters $\theta$ are iteratively updated using the proposed QHEA until the reconstructed accelerations agree well with the measured values.

## 3. Identification algorithms

Heuristic algorithms have been widely adopted as the search tool to deal with the optimization-based damage detection problem. Considering the complex nonlinear characteristic of optimization problem, more various optimization algorithms are welcomed.

### 3.1. Jaya algorithm

In recent years, a new Jaya algorithm is proposed [45]. The population of Jaya algorithm is initialized randomly within the given search domain

$$\begin{aligned} X_{i,j}^{\text{initial}} &= Lb_{i,j} + rand(0,1) \times \left(Ub_{i,j} - Lb_{i,j}\right) \\ i &\in (1,2,...,NP), \quad j \in (1,2,...,Dim) \end{aligned} \tag{20}$$

where $X_{i,j}^{\text{initial}}$ denotes the *j*-th variable of the *i*-th individual in the initial population; $Lb_{i,j}$ and $Ub_{i,j}$ means the lower and upper search limits; *NP* and *Dim* represent population size and dimension of variables, respectively; $rand(0,1)$ stands for a random number with uniform distribution within the range of [0, 1];

Then, at the *G*-th iteration, new candidate solutions $X_{i,G}^{'}$ is updated with the best solution $X_{best,G}$ and the worst solution $X_{worst,G}$ as follows

$$\begin{aligned} X_{i,j,G}^{'} = \; & X_{i,j,G} + rand_1 \times \left(X_{best,j,G} - \left|X_{i,j,G}\right|\right) \\ & - rand_2 \times \left(X_{worst,j,G} - \left|X_{i,j,G}\right|\right) \end{aligned} \tag{21}$$

where $X_{i,j,G}$ stands for the *j*-th variable of the *i*-th individual; $rand_1$ and $rand_2$ are two uniformly random number within [0, 1].

Subsequently, greedy selection mechanism is applied as follows

$$X_{i,G+1} = \begin{cases} X_{i,G}^{'} & f_{obj}\left(X_{i,G}^{'}\right) \leqslant f_{obj}\left(X_{i,G}\right) \\ X_{i,G} & otherwise \end{cases} \tag{22}$$

where $f_{obj}(X_{i,G})$ and $f_{obj}(X_{i,G}^{'})$ are the objective functions of the solution $X_{i,G}$ and $X_{i,G}^{'}$.

Finally, the best solution will be output if the termination condition is satisfied.

### 3.2. Differential evolution algorithm

DE algorithm has been widely applied into various fields in recent years. The initial population $(X_1, X_2, ..., X_{NP})$ is produced randomly using Eq. (20). Then, mutation individual $V_{i,G}$ is generated with mutation operation. There are several commonly referred mutation strategies, such as DE/rand/1, DE/rand/2, DE/best/1, DE/best/2, DE/rand-to-best/1, DE/current-to-best/1. Herein, taking the basic DE/rand/1 for example, its expression is

$$V_{i,G} = X_{r_1,G} + F\left(X_{r_2,G} - X_{r_3,G}\right) \tag{23}$$

where $X_{r_1,G}, X_{r_2,G}, X_{r_3,G}$ stand for randomly selected target individuals, $r_1 \neq r_2 \neq r_3 \neq i$; mutation operator *F* is generally set as 0.8, which controls the deviation of difference vector.

After mutation, to create trial individual $U_{i,G}$, binomial crossover strategy is utilized by crossing the mutated individual $V_{i,G}$ and the original target individual $X_{i,G}$

$$U_{i,j,G} = \begin{cases} V_{i,j,G} & if\left(rand_j[0, \quad 1] \leqslant CR\right) or (j = j_{rand}), \quad j = 1,2,...,Dim \\ X_{i,j,G} & otherwise \end{cases} \tag{24}$$

where $rand_j[0, \quad 1]$ denotes a random number within the range of [0, 1]; $j_{rand}$ stands for an integer number within [1, *Dim*]; *CR* is the crossover operator usually chosen as 0.9 [50].

In the last step, greedy selection mechanism is employed to select better candidate solution between $X_{i,G}$ and $U_{i,G}$ using Eq. (22).

### 3.3. Q-learning hybrid evolutionary algorithm

#### 3.3.1. Strategy pool

It is well-known that essential roles are played by exploration and exploitation in the search processes of evolutionary algorithm toward optimization and/or convergence. The tradeoff between exploration and exploitation is the key factor determining the performance of any given evolutionary algorithm. The former refers to visiting the new regions within the predefined search domain, while the latter is defined as visiting those regions around the previously visited points. In fact, a paradox exists behind these two search modes. If much attention is paid to the exploration mode, the convergence performance of evolutionary algorithm would be weakened. On the contrary, if it concentrates on the exploitation mode, this algorithm may fall into local optimum. Some studies have been done to achieve a balanced exploration and exploitation capacities by introducing diverse mechanisms, k-means clustering technique, mutation learning mechanism, experience-based learning strategy, etc. In consideration of the strengths and weaknesses of different search strategies, in this study, strategy pool method including four different search strategies, DE/rand/1, DE/rand/2, DE/current-to-best/1, Jaya mutation is proposed, expressed as following equation

$$Strategy\ pool = \begin{cases} Group_1 \begin{cases} DE/rand/1 \\ DE/rand/2 \end{cases} \\ Group_2 \begin{cases} DE/current-to-best/1 \\ Jaya\ mutation \end{cases} \end{cases} \tag{25}$$

In Eq. (25), the proposed strategy pool has exploration group $Group_1$ and exploitation group $Group_2$. $Group_1$ consists of DE/rand/1 and DE/rand/2, and it ensures this strategy's exploration capability; $Group_2$ consists of DE/current-to-best/1 and Jaya mutation, which ensures this strategy's exploitation capacity. The Eq. (25) can be rewritten as

$$\begin{cases} \begin{cases} V_{i,G} = X_{r_1,G} + F\left(X_{r_2,G} - X_{r_3,G}\right) \\ V_{i,G} = X_{r_1,G} + F\left(X_{r_2,G} - X_{r_3,G}\right) + F\left(X_{r_4,G} - X_{r_5,G}\right) \end{cases} \\ \begin{cases} V_{i,G} = X_{i,G} + F\left(X_{best,G} - X_{i,G}\right) + F\left(X_{r_1,G} - X_{r_2,G}\right) \\ V_{i,j,G} = X_{i,j,G} + rand_1 \times \left(X_{best,j,G} - \left|X_{i,j,G}\right|\right) - rand_2 \times \left(X_{worst,j,G} - \left|X_{i,j,G}\right|\right) \end{cases} \end{cases} \tag{26}$$

$Group_1$ has strong global exploration capacity and $Group_2$ features powerful local exploitation capacity. The combination of these four search strategies may provide more balanced capacity between exploration and exploitation.

### 3.3.2. Q-learning algorithm

As a branch of artificial intelligence, reinforcement learning has been widely employed into various fields [51]. The main components of reinforcement learning, as presented in Fig. 1, are environment, state, reward, agent and action. The operations of reinforcement learning process are composed of the cycles of state, action and reward.

Q-learning is one of the most well-known algorithms of reinforcement learning, adopted in this study, and its introduction is briefly described. Q-learning algorithm consists of a set of states of the environment $S = \{s_1, s_2, ..., s_n\}$ and actions $A = \{a_1, a_2, ..., a_n\}$ to be implemented. At each iteration, an intelligent agent with state $s_t$ would perform the best action based on an accumulated table of information, Q-table. Then, a reward $w_{t+1}$ and a new state $s_{t+1}$ are obtained. The agent learns the obtained information to form evaluations of expected values $Q(s_t, a_t)$ obtained by each given action [52]. The Q-learning estimates the value of $Q(s_t, a_t)$ according to following Bellman equation

$$\begin{aligned} Q^{new}(s_t, a_t) = \ & (1-\varphi)Q(s_t, a_t) \\ & +\varphi[w_{t+1} + \gamma \cdot \max Q(s_{t+1}, a_t)] \end{aligned} \tag{27}$$

where $Q(s_t, a_t)$ and $Q^{new}(s_t, a_t)$ stand for the previous and updated Q-values; $\max Q(s_{t+1}, a_t)$ is the maximum Q-value among all actions; $\gamma$ means the discount factor, usually set as $\gamma = 0.8$; $w_{t+1}$ denotes the immediate reward received from the environment by taking action $a$; $\varphi$ is the learning rate. Normally, in the early stage, it has a high value and decreased with iterations

$$\varphi_t = 1 - 0.9 \times \frac{Iter}{Max\_Iter} \tag{28}$$

where $Iter$ and $Max\_Iter$ are the current iteration number and the maximum iterations.

### 3.3.3. Framework of Q-learning hybrid evolutionary algorithm

In this section, a novel algorithm, Q-learning hybrid evolutionary algorithm (QHEA), is proposed by integrating the strategy pool in Section 3.3.1 and the Q-learning algorithm in Section 3.3.2 together. More specifically, the individuals of evolutionary algorithm refer to the intelligent agents of reinforcement learning. The environment is defined as the predefined search space limits of the individuals. The states stand for the possible operations for each individual of hybrid algorithm, namely, DE/rand/1, DE/rand/2, DE/current-to-best/1, Jaya mutation. The action implies it changes from one state to another. The individual is switched by Q-learning algorithm in a self-adaptive manner from one operation (state) to another in the light of the individual's achievement. Positive rewards and negative rewards are given to the individuals with good performance and poor behavior, respectively.

The optimization process of the proposed QHEA can be further summarized as following several phases:

Phase 1: the initial population of evolutionary algorithm is generated with Latin hypercube sampling.

Phase 2: a 4 × 4 matrix $Q(s_t, a_t)$ is randomly produced as initial Q-table for each individual. The dimension of matrix $Q$ is the number of states, i.e., DE/rand/1, DE/rand/2, DE/current-to-best/1 and Jaya mutation.

Phase 3: for the current individual, the best action would be selected on the basis of the position of the maximum Q-value in the Q-table as follows

$$best\ action = Max[Q(current\ \ state,\ \ \ all\ \ \ actions)] \tag{29}$$

Phase 4: perform the selected operation and calculate the objective function.

Phase 5: determine the reward/penalty according to whether the solution improved or not [53]

$$w_t = \begin{cases} 1 & if\ \ f_{obj}\ \ is\ \ improved \\ -1 & otherwise \end{cases} \tag{30}$$

Phase 6: update the Q-table for the current individual by Eq. (27).

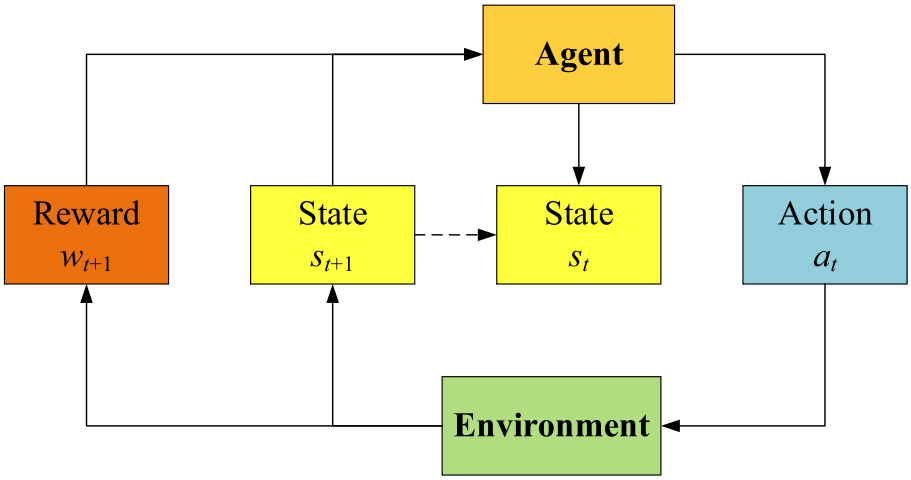


**Fig. 1.** The standard reinforcement learning model.

Phase 7: repeated the procedures until the termination condition is met.

Fig. 2 presents the pseudo-code of the proposed QHEA. The most suitable search strategy for each individual is adaptively selected based on the Q-learning algorithm. The tradeoff between exploration and exploitation of QHEA would be better achieved than Jaya and DE.

### 3.4. Iterative identification procedure

Fig. 3 presents the flowchart of the proposed output-only approach based on QHEA and response reconstruction technique for identifying structural damages with unknown excitation force, and its procedures are illustrated as follows.

Step 1: acquire the dynamic acceleration response from the damaged structure and divide these measured data into two different sets $\ddot{u}_{mea}^{set1}(t)$ and $\ddot{u}_{mea}^{set2}(t)$. Initialize the population and parameters of QHEA.

Step 2: after calculating the unit impulse response function, matrices $H_1$ and $H_2$ associated with unknown structural parameters $\theta_i$ can be obtained by Eq. (10) or Eq. (18).

Step 3: the reconstructed responses of measurement set 2 $\ddot{u}_{rec}^{set2}(t)$ can be calculated with Tikhonov regularization technique and the transformation matrix $T_{12}$ using Eq. (15).

Step 4: calculate the objective function based on the measured and reconstructed responses of set 2 with Eq. (19).

Step 5: iteratively update the unknown structural parameters $\theta_i$ using the proposed QHEA.

Step 6: repeat steps 2 to 5 until the predefined maximum iterations reached or following convergence criteria is satisfied

$$error_G = \frac{\left\|\theta_{i,G+1} - \theta_{i,G}\right\|_2}{\left\|\theta_{i,G}\right\|_2} \times 100\% \leqslant Tolerance \tag{31}$$

where *Tolerance* means the convergence tolerance, taken as $5 \times 10^{-3}$ in this study.

Step 7: output the optimal solution, so the locations and extents of structural damages can be identified.

## 4. Numerical studies

To examine the superiority of the proposed QHEA, CEC2005 benchmark tests are employed. In addition, a cantilever beam structure and a truss structure are used as numerical examples to test the performance of the proposed output-only damage detection approach under single force or multiple input excitations, respectively.

### 4.1. CEC2005 benchmark tests

Some representative CEC2005 benchmarks functions, such as unimodal functions (F1, F2, F3, F4, F5), multimodal biased functions (F6, F7, F9, F10, F11, F12), and expanded functions (F13, F14), are adopted to conduct verification. Compared with classical benchmarks, such as Sphere, Griewank, Ackley, CEC2005 benchmarks functions are more complex to be well optimized owing to their shifted global optimum, hybridization, expansion features. Thus, the significance of CEC 2005 benchmark functions is that they can be employed as an effective tool to test the performance of the proposed QHEA algorithm. The results from four state-of-the-art algorithms including evolutionary

Set maximum iterations *Max_Iter*, population size *NP*, number of variables to be identified *Dim*, mutation operator and crossover operator, the upper and lower search limits
Generate an initial population using Latin hypercube sampling method within the predefined search space
Randomly produced a $4 \times 4$ matrix $Q$ as initial Q-table
Initialize iteration number $Iter = 1$
**While** termination criterion is not reached **Do**
  **For** all individual $X_i$ in the population
    Evaluate the objective function for each candidate
    Sort objective function values and determine the best and the worst solutions
    Select the best action $a_t$ for the current state $s_t$ by the location of the maximum Q-value in the Q-table
    **Switch action**
      **Case 1**
        Update solution with DE/rand/1
        Implement crossover operation
      **Case 2**
        Update solution with DE/rand/2
        Implement crossover operation
      **Case 3**
        Update solution with DE/current-to-best/1
        Implement crossover operation
      **Case 4**
        Update solution with Jaya mutation
  **End for**
  Evaluate the objective function of updated solution
  **For** individual $i = 1$ to $NP$
    Individual with better solution will survive according to greedy selection mechanism
    Obtain the immediate reward using Eq. (30)
    Determine the maximum Q-value for the next state $s_{t+1}$
    Update the Q-table with Eq. (27)
    Update the current state $s_t = s_{t+1}$
  **End for**
  $Iter = Iter + 1$
**End while**
Output the global best solution

**Fig. 2.** The pseudo-code of proposed QHEA.

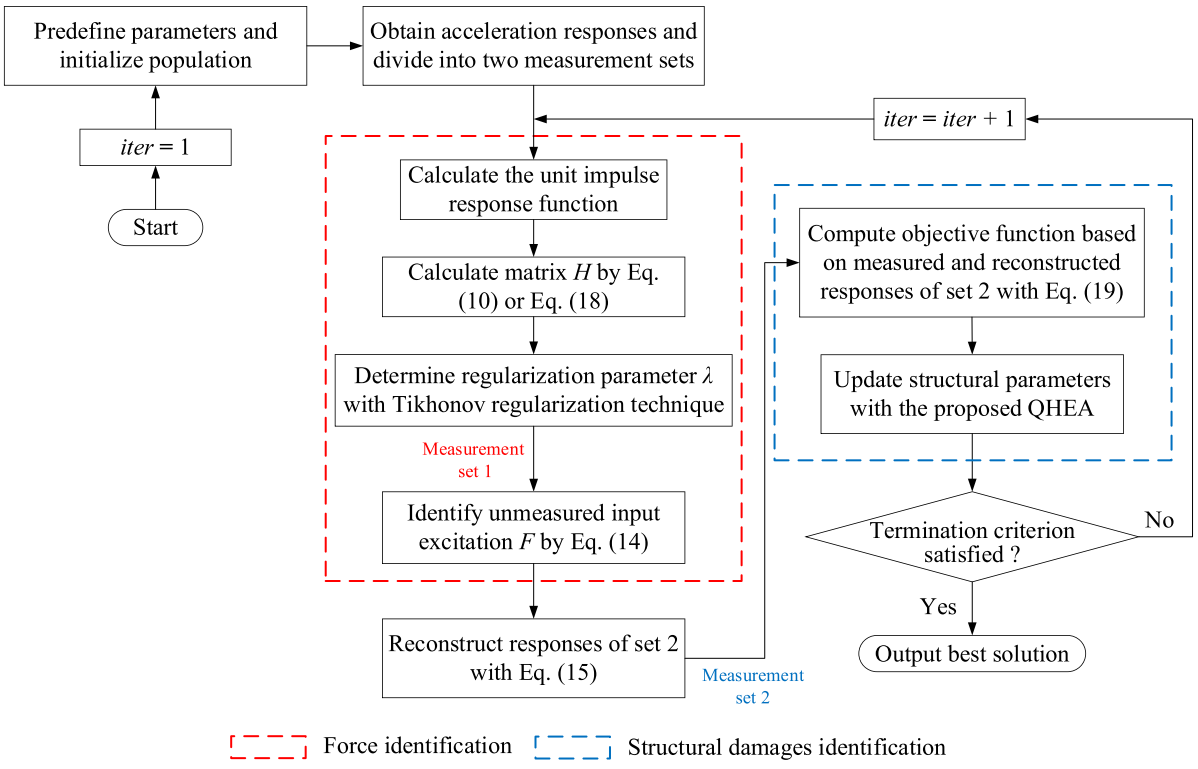


**Fig. 3.** The flowchart of the proposed method.

sampling assisted optimization algorithm (ESAO) [54], improved global-best harmony search (IGHS) [55], modified particle swarm optimization (MPSO) [56], surrogate-assisted multiswarm optimization algorithm (SAMSO) [57], are cited for comparison with QHEA. The statistical results from 30 independent runs for the 30 and 50-dimensional tests are presented in Table 1 and Table 2, respectively. It is noted that the bold value means the best identified value among these five algorithms. By Table 1 and Table 2, it can be easily found that the proposed QHEA can obtain more pleasant results than ESAO, IGHS, MPSO, SAMSO in most cases. In addition, the well-known non-parametric Friedman test on the CEC2005 benchmark function is conducted to rank these algorithms from a statistical point of view. Fig. 4 shows the mean ranks of ESAO, IGHS, MPSO, SAMSO, QHEA. The proposed QHEA obtains the best rank with 1.54 for D = 30 and 1.23 for D = 50.

### 4.2. Cantilever beam structure under single excitation

To validate the effectiveness of the proposed output-only damage detection approach, a Euler–Bernoulli cantilever beam structure, as shown in Fig. 5, is taken as the first numerical example. The total length is 1500 mm, and width and height of rectangular cross-section are 50.75 mm and 6 mm. The cantilever beam is evenly discretized into 15 elements, so the length of each element is 100 mm. Vertical translation and rotation are considered for each node. The elastic modulus and mass density of steel material are 210 GPa and 7860 kg/m$^3$, respectively. For the Rayleigh damping model, 1 % damping ratio is set. The cantilever beam is subjected to a random white noise excitation at node 16 in the vertical direction. Five accelerometers are installed at nodes 4, 7, 9, 11, 13 to record the vertical responses, as presented in Fig. 5, and they are divided into two sets. The vertical accelerations from nodes 9, 11, 13 are regarded as the measurement set 1, and the acceleration measurements from nodes 4, 7 are denoted as the measurement set 2. The sampling rate

**Table 1**
Comparison of results of ESAO, IGHS, MPSO, SAMSO, QHEA on CEC2005 benchmark functions (30D).

| Num | ESAO | | IGHS | | MPSO | | SAMSO | | QHEA | |
|---|---|---|---|---|---|---|---|---|---|---|
| | Mean | Std. | Mean | Std. | Mean | Std. | Mean | Std. | Mean | Std. |
| F1 | 2.66E-04 | 5.18E-05 | 8.87E-08 | 1.25E-08 | 3.22E-14 | 2.86E-14 | 4.16E-05 | 1.72E-05 | **1.64E-16** | **1.19E-16** |
| F2 | 4.83E + 04 | 9.90E + 03 | **6.51E-07** | **1.68E-07** | 4.72E-01 | 6.45E-01 | 2.12E + 04 | 5.54E + 03 | 1.75E-04 | 3.46E-04 |
| F3 | 1.10E + 08 | 5.07E + 07 | 4.78E + 05 | 2.36E + 05 | 4.89E + 06 | 6.73E + 06 | 2.78E + 07 | 9.07E + 06 | **1.42E + 05** | **3.86E + 04** |
| F4 | 1.00E + 05 | 2.54E + 04 | 9.59E-03 | 1.89E-02 | 6.22E + 02 | 4.20E + 02 | 3.48E + 04 | 5.15E + 03 | **3.97E-03** | **1.14E-03** |
| F5 | 2.92E + 04 | 2.17E + 03 | 1.18E + 03 | 5.32E + 02 | 3.84E + 03 | 8.32E + 02 | 6.94E + 03 | 1.54E + 03 | **5.76E + 02** | **4.76E + 01** |
| F6 | 2.65E + 04 | 2.90E + 04 | **1.61E + 02** | 1.71E + 02 | 2.93E + 06 | 6.09E + 06 | 5.57E + 07 | 1.78E + 07 | 7.95E + 02 | **2.61E + 01** |
| F7 | 4.70E + 03 | **5.13E-07** | **8.70E-03** | 1.06E-02 | 7.66E-01 | 3.69E + 00 | 4.70E + 03 | 3.45E-06 | 7.43E-02 | 1.86E-01 |
| F9 | 2.40E + 02 | 2.27E + 01 | **1.69E-05** | **1.70E-06** | 4.34E + 01 | 1.49E + 01 | 7.88E + 01 | 1.92E + 01 | 9.13E-03 | 4.79E-04 |
| F10 | 2.94E + 02 | 2.65E + 01 | 4.98E + 01 | **1.41E + 01** | 8.60E + 01 | 2.73E + 01 | 9.35E + 01 | 2.37E + 01 | **1.03E + 01** | 1.52E + 01 |
| F11 | 4.60E + 01 | **1.75E + 00** | 5.60E + 00 | 2.25E + 00 | 2.47E + 01 | 4.31E + 00 | 3.34E + 01 | 4.97E + 00 | **2.36E + 00** | 2.46E + 00 |
| F12 | 3.74E + 04 | 3.94E + 04 | 1.59E + 03 | 1.74E + 03 | 5.35E + 04 | 2.87E + 04 | 4.04E + 04 | 2.46E + 04 | **1.25E + 03** | **7.16E + 01** |
| F13 | 4.14E + 01 | 1.25E + 01 | **1.23E + 00** | **2.43E-01** | 2.73E + 00 | 6.84E-01 | 6.66E + 01 | 2.83E + 01 | 2.84E + 00 | 8.17E-01 |
| F14 | 1.42E + 02 | 1.85E-01 | 1.19E + 01 | 5.73E-01 | 1.28E + 01 | 3.87E-01 | **1.40E + 00** | **1.39E-01** | 1.08E + 01 | 2.19E-01 |
| Rank | 4.58 | | 1.77 | | 3.15 | | 3.96 | | **1.54** | |

**Table 2**
Comparison of results of ESAO, IGHS, MPSO, SAMSO, QHEA on CEC2005 benchmark functions (50D).

| Num | ESAO | | IGHS | | MPSO | | SAMSO | | QHEA | |
|---|---|---|---|---|---|---|---|---|---|---|
| | Mean | Std. | Mean | Std. | Mean | Std. | Mean | Std. | Mean | Std. |
| F1 | 3.14E-02 | 1.19E-02 | 2.74E-07 | 2.87E-08 | 1.13E + 03 | 2.70E + 03 | 6.47E-04 | 3.24E-04 | **2.07E-16** | **2.73E-18** |
| F2 | 1.91E + 05 | 3.20E + 04 | **9.63E-06** | **1.92E-06** | 1.73E + 02 | 7.26E + 02 | 6.94E + 04 | 1.19E + 04 | 1.19E-04 | 3.75E-04 |
| F3 | 3.97E + 08 | 1.78E + 08 | 9.07E + 05 | 3.72E + 05 | 4.59E + 07 | 5.19E + 07 | 1.14E + 08 | 2.67E + 07 | **3.16E + 05** | **1.07E + 05** |
| F4 | 2.51E + 05 | 4.32E + 04 | 3.18E + 03 | 2.03E + 03 | 1.30E + 04 | 4.36E + 03 | 9.67E + 04 | 1.73E + 04 | **3.75E-01** | **8.13E-01** |
| F5 | 1.73E + 04 | 2.90E + 03 | 3.29E + 03 | 7.67E + 02 | 8.62E + 03 | 1.69E + 03 | 1.66E + 04 | 3.05E + 03 | **4.17E + 02** | **1.34E + 01** |
| F6 | 1.27E + 04 | 8.85E + 03 | 1.45E + 02 | 1.70E + 02 | 5.60E + 07 | 6.97E + 07 | 2.56E + 08 | 7.77E + 07 | **1.26E + 00** | **5.68E-01** |
| F7 | 6.20E + 03 | **5.22E-06** | **1.07E-03** | 2.80E-03 | 1.06E + 03 | 7.25E + 02 | 6.20E + 03 | 1.03E-04 | 3.52E-02 | 7.46E-04 |
| F9 | 4.75E + 02 | 2.71E + 02 | 5.12E-05 | 4.33E-06 | 8.02E + 01 | 2.16E + 01 | 1.54E + 02 | 4.83E + 01 | **8.57E-09** | **6.82E-09** |
| F10 | 5.29E + 02 | 4.58E + 01 | 8.94E + 01 | 2.13E + 01 | 1.70E + 02 | 4.76E + 01 | 1.87E + 02 | 4.61E + 01 | **1.81E + 01** | **1.63E + 01** |
| F11 | 8.22E + 01 | 1.78E + 00 | 1.20E + 01 | 3.35E + 00 | 5.13E + 01 | 4.41E + 00 | 6.41E + 01 | 8.31E + 00 | **3.68E-01** | **9.04E-01** |
| F12 | 1.59E + 05 | 5.01E + 04 | 1.22E + 04 | 1.04E + 04 | 3.58E + 05 | 1.34E + 05 | 2.61E + 05 | 9.83E + 04 | **1.12E + 04** | **3.20E + 03** |
| F13 | 5.38E + 01 | 8.82E + 00 | **2.01E + 00** | **2.83E-01** | 6.03E + 00 | 1.54E + 00 | 6.14E + 02 | 4.47E + 02 | 5.42E + 00 | 3.04E + 01 |
| F14 | 2.42E + 01 | 1.58E-01 | 2.11E + 01 | 7.82E-01 | 2.25E + 01 | 4.69E-01 | 2.39E + 01 | **1.48E-01** | **1.03E + 01** | 1.54E-01 |
| Rank | 4.50 | | 1.77 | | 3.38 | | 4.12 | | **1.23** | |

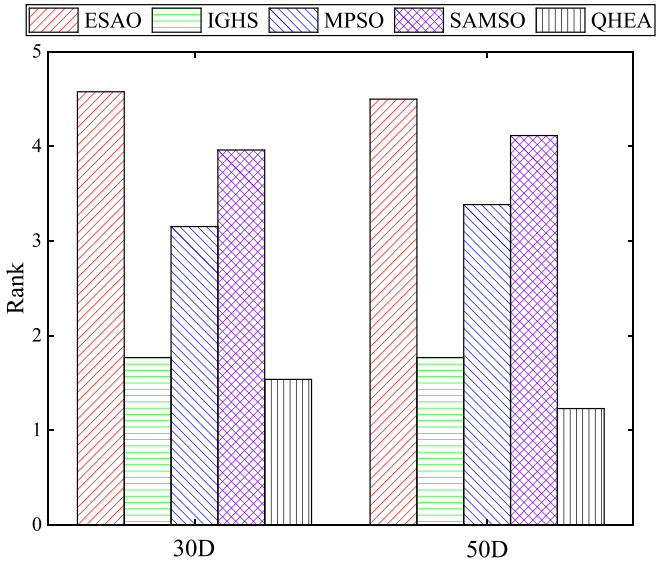


**Fig. 4.** The results of Friedman rank test for CEC2005 benchmark functions.

is set as 1000 samples/s and 1 s vibration data are selected for response reconstruction and damage identification.

A random component is added into clean acceleration responses to simulate measurement noise by

$$\ddot{u}_{mea}(t) = \ddot{u}_{clean}(t) + N_l N_{noise} RMS\left(\ddot{u}_{clean}(t)\right) \tag{32}$$

where $\ddot{u}_{clean}(t)$ and $\ddot{u}_{mea}(t)$ are the clean and noise contaminated acceleration responses; $N_l$ stands for the level of noise; $N_{noise}$ denotes the randomly generated noise vector with mean value of 0 and standard deviation of 1; $RMS\left(\ddot{u}_{clean}(t)\right)$ means the root mean square of the corresponding structural response.

#### 4.2.1. Response reconstruction

If the FE model of cantilever beam is known, the reconstructed accelerations in measurement set 2 can be directly calculated with the aid of response reconstruction and Tikhonov regularization techniques. Fig. 6 presents the comparison of measured response $\ddot{u}^{set2}_{mea}(t)$ and reconstructed acceleration responses $\ddot{u}^{set2}_{rec}(t)$ of the set 2 for noise-free case. It is obviously observed from Fig. 6(a) and Fig. 6(c) that the reconstructed responses match well with the measured values. By Fig. 6(b) and Fig. 6(d), the amplitude of errors between the measured and reconstructed accelerations of node 4 and node 7 are less than $4 \times 10^{-12}$ and $15 \times 10^{-12}$, respectively, which indicates the accuracy of response reconstruction method. When contaminated with 5 % noise, similarly, as presented in Fig. 7(a) and Fig. 7(c), the reconstructed accelerations are quite consistent with the measured ones. By Fig. 7(b) and Fig. 7(d), the errors of measurements from nodes 4 and 7 are less than 0.4. To evaluate the quality of response reconstruction, two quantitative indicators are adopted as follows

$$RE = \frac{\left\| \ddot{u}^{set2}_{mea} - \ddot{u}^{set2}_{rec} \right\|_2}{\left\| \ddot{u}^{set2}_{mea} \right\|_2} \times 100\% \tag{33}$$

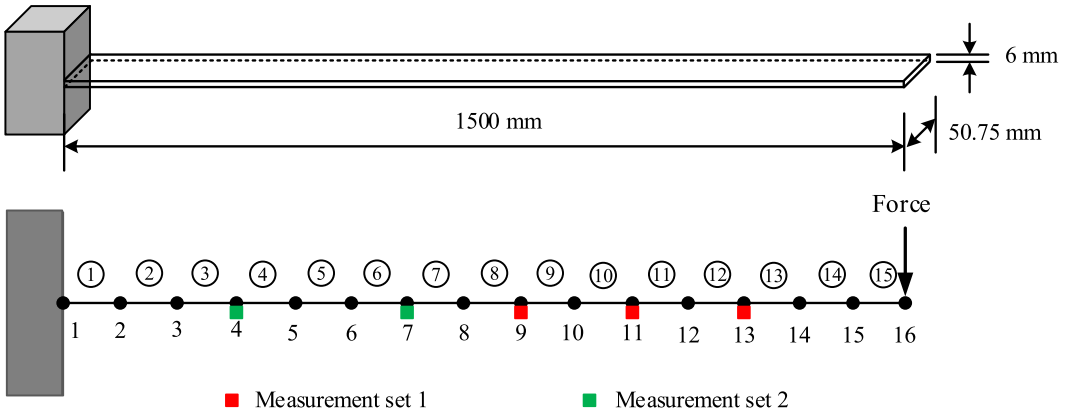


**Fig. 5.** The FE model of cantilever beam structure.

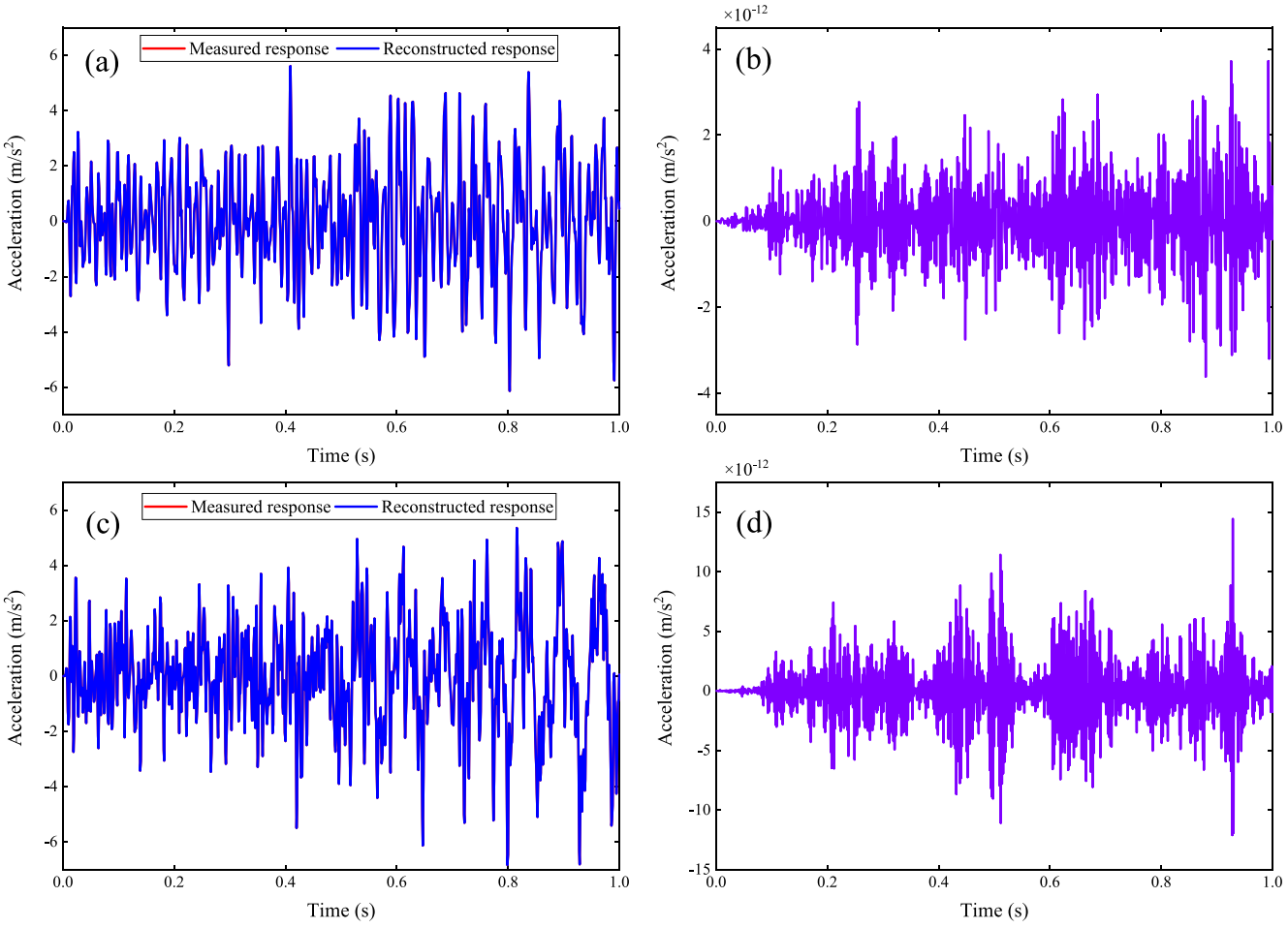


**Fig. 6.** Comparison of measured and reconstructed acceleration responses of the measurement set 2 without measurement noise: (a) response at node 4; (b) error of reconstructed acceleration at node 4; (c) response at node 7; (d) error of reconstructed acceleration at node 7.

$$PCC\left(\ddot{u}_{mea}^{set2}, \ddot{u}_{rec}^{set2}\right) = \frac{cov\left(\ddot{u}_{mea}^{set2}, \ddot{u}_{rec}^{set2}\right)}{\sigma_{\ddot{u}_{mea}^{set2}} \sigma_{\ddot{u}_{rec}^{set2}}} \tag{34}$$

where *cov* represents the covariance and $\sigma$ stands for the standard deviation of acceleration response.

By Eqs. (33–34), relative error (*RE*) means the deviation and Pearson correlation coefficient (*PCC*) shows the linear correlation degree. Table 3 provides the results of *RE* and *PCC* under 0 %, 5 % and 10 % noises. It is found that excellent accuracy of structural response reconstruction can be acquired.

Besides, the unknown input force is reconstructed and compared with the accurate value without and with 10 % noise, as shown in Fig. 8. Some deviations can be observed in time domain, while the frequency component of the identified unknown force within the range of [1, 400] in frequency domain agrees well with the true value, which implies the unknown input excitation can be successfully identified via response reconstruction technique.

#### 4.2.2. Damage identification

According to the iterative identification procedures in Section 3.4, the proposed output-only approach making use of QHEA and response reconstruction technique is employed to identify structural damage identification. Assuming there are 20 % and 15 % reductions of stiffness at the 8th and 12th elements, namely, $\alpha_8 = 0.2, \alpha_{12} = 0.15$. The optimal regularization parameters $\lambda_{op}$ under 0 %, 5 %, 10 % noise are $1.06 \times 10^{-12}$, 0.0094, 0.0102, respectively. The population size *NP* and maximum iterations *Max_Iter* of the proposed QHEA are 100 and 200, respectively. To ensure the effectiveness, the average values of five independent runs are taken as the final results.

Fig. 9 depicts the damage identification results under 0 %, 5 %, 10 % measurement noise, and Table 4 lists the final mean errors and maximum errors. For the noise-free case, it is easily observed that the locations and extents of the structural damages are accurately identified. More specifically, the identified damage extents of the 0 % noise case at elements 8 and 12 are 19.94 % and 14.99 %. The identified damage extents of the 5 % noise case at elements 8 and 12 are 17.39 % and 15.78 %. For the case of 10 % noise, 5.43 % maximum error is noticed at element 11 possibly owing to the errors of response reconstruction. Besides, the adverse effect of modeling errors on the accuracy of damage detection is investigated. Herein, 1 % uncertainty with Gaussian distributions is added into the stiffness parameters for all elements to consider the modeling errors in numerical structure [58]. Fig. 10 presents the identified damage extent with modeling errors. The damage extents at elements 8 and 12 are identified as 20.01 % and 15.00 % with noise-free, 18.71 % and 15.13 % with 5 % noise. When contaminated with 10 % noise, the damage location of element 12 is detected, while 5.38 % identification error at element 12 and around 4 % false identification at element 15 are observed, which implies the negative effect of modeling errors and measurement noise on damage identification results. These results demonstrate that the proposed output-only approach is able to accurately detect structural damages even contaminated with 10 % noise.

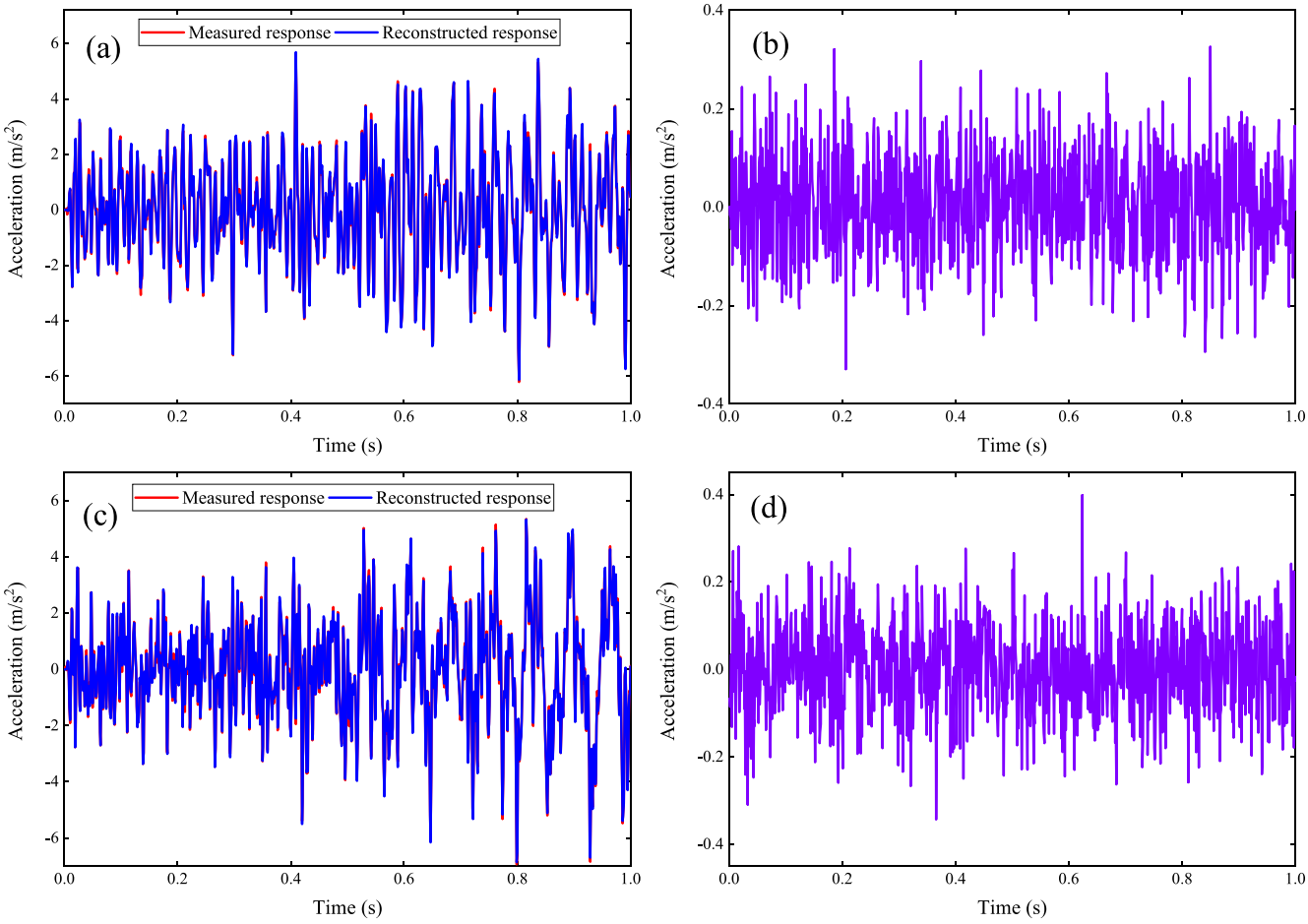


**Fig. 7.** Comparison of measured and reconstructed acceleration responses of the measurement set 2 with 5% noise: (a) response at node 4; (b) error of reconstructed acceleration at node 4; (c) response at node 7; (d) error of reconstructed acceleration at node 7.

**Table 3**
Percentage errors of the reconstructed responses of measurement set 2.

| Type of reconstruction | 0 % noise | | 5 % noise | | 10 % noise | |
|---|---|---|---|---|---|---|
| | *RE* | *PCC* | *RE* | *PCC* | *RE* | *PCC* |
| Acceleration response at node 4 | 0 | 1 | 5.43 | 0.9985 | 10.46 | 0.9942 |
| Acceleration response at node 7 | 0 | 1 | 5.46 | 0.9985 | 10.48 | 0.9945 |

### 4.3. Truss structure under multiple excitations

A two-dimensional truss structure under multiple input excitations is used as the second example. Fig. 11 presents the numerical model. The simply-supported truss structure consists of 22 nodes, 51 elements and 41 DOFs in total. The boundary conditions are considered as a pin support at node 1 and a roller support at node 22. The height and length of the truss structure are 2 m and 20 m. The elastic modulus and density of steel material are 210 GPa and 7850 kg/m$^3$, respectively. The cross-sectional area 0.0016 m$^2$ is identical for each element. Three Gaussian random excitations with amplitude of 200 N are applied at nodes 5, 11, 15 in the vertical direction. There are six accelerometers installed on the structure, as shown in Fig. 11, to record the vertical acceleration responses. These acceleration responses are divided into two measurement sets in order to carry out the response reconstruction technique. The vertical accelerations responses from nodes 7, 12, 16, 17 are named as the measurement set 1, and the acceleration measurements from nodes 6, 13 are regarded as the measurement set 2. In this study, 0.5 s vibration responses are recorded with a sampling rate of 1000 samples/s, used for the subsequent investigations of response reconstruction and damage identification.

#### 4.3.1. Identification with QHEA

Assuming there are 30 %, 20 % and 15 % reductions of stiffness at the 15th, 33th, 42th, elements, namely, $\alpha_{15} = 0.3, \alpha_{33} = 0.2, \alpha_{42} = 0.15$. In the proposed QHEA, population size *NP* and maximum iterations *Max_Iter* are 100 and 400, respectively. The tolerance of convergence criteria in Eq. (31) is set as $5 \times 10^{-3}$. The optimal regularization parameters $\lambda_{op}$ for 0 %, 5 %, 10 % noise cases are calculated as $9.2 \times 10^{-6}$, $2.6 \times 10^{-3}$, 0.018, respectively.

The acceleration responses of set 2 are reconstructed based on the responses of measurement set 1 and impulse response function matrix. Fig. 12(a) and Fig. 12(c) provide the measured acceleration and reconstructed one of node 13. For the case of noise free, less than $8 \times 10^{-14}$ error is observed in Fig. 12(b), which proves the excellent consistency between the reconstructed response and the simulated measured response. When contaminated with 5 % noise, the reconstructed response in Fig. 12(d) can still accurately approach the actual one with a value of less than 0.03. Three different levels of noise, i.e., 0 %, 5 %, 10 % are considered to validate the robustness. Fig. 13 shows the identified damage extents using QHEA with 0 % noise, 5 % noise and 10 % noise corresponding to Fig. 13(a), Fig. 13(b) and Fig. 13(c), respectively. It can be found that pleasant identification results are achieved with the mean errors of 0.06 %, 0.31 %, 0.88 %, as well as the maximum errors of 1.85 %, 2.95 %, 5.14 %, corresponding to the cases of 0 % noise, 5 % noise, 10 % noise. Furthermore, Fig. 14 shows the

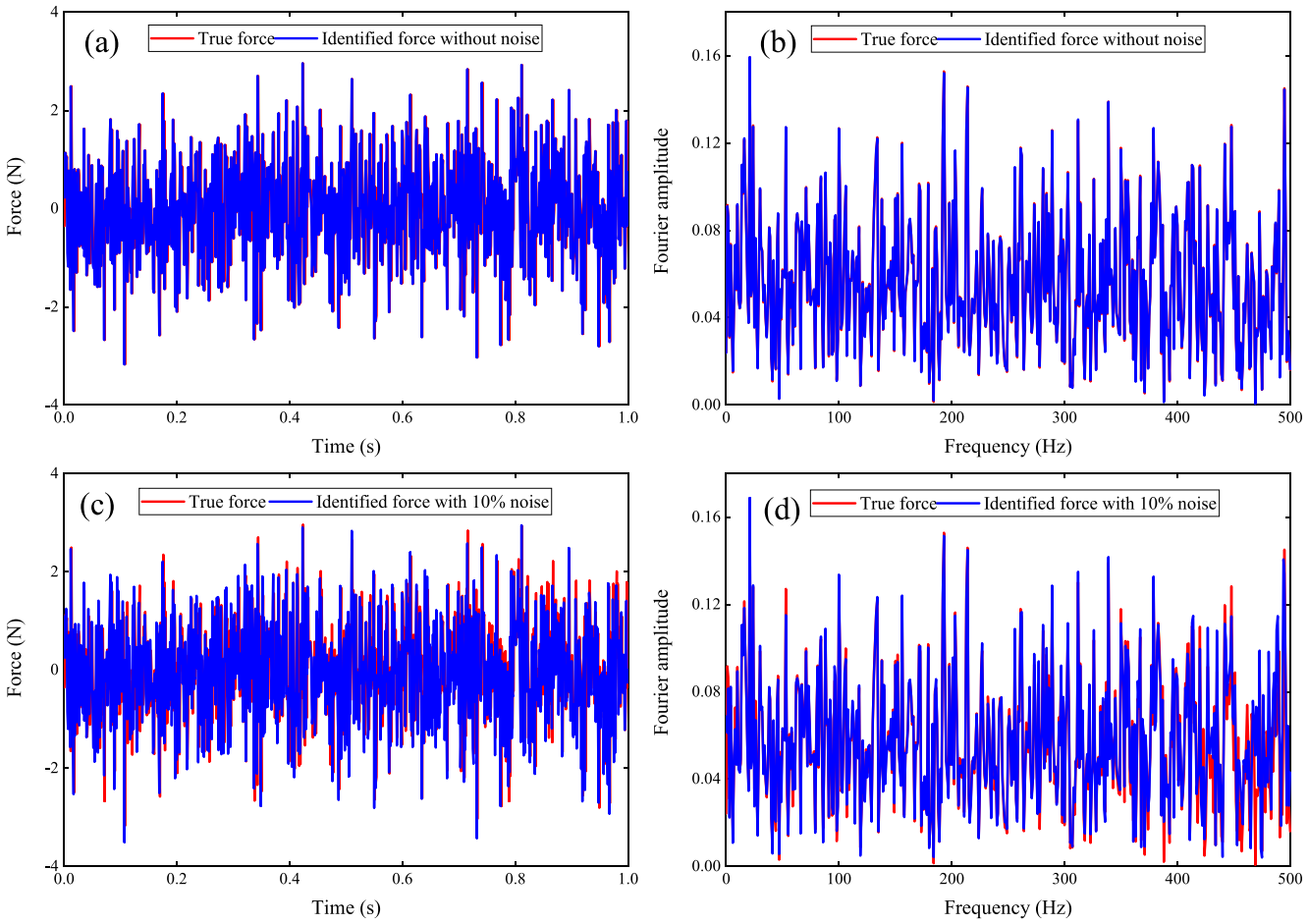


**Fig. 8.** Comparison of the identified force with true force: (a) time history without noise; (b) frequency spectrum without noise; (c) time history with 10% noise; (d) frequency spectrum with 10% noise.

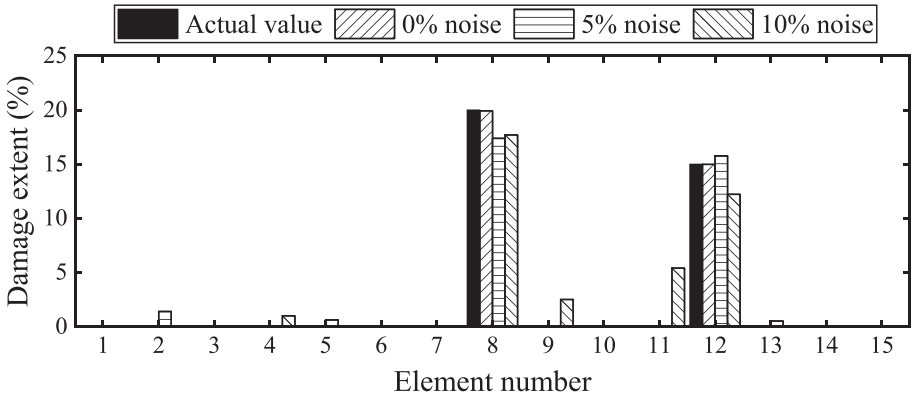


**Fig. 9.** Damage identification results with different levels of noise.

**Table 4**
The identified errors of beam structure without and with modeling errors (%).

| Cases | Noise free | | 5 % noise | | 10 % noise | |
|---|---|---|---|---|---|---|
| | Mean error | Max error | Mean error | Max error | Mean error | Max error |
| Without modeling error | 0.01 | 0.06 | 0.40 | 2.61 | 0.93 | 5.43 |
| With modeling error | 0.84 | 2.89 | 0.95 | 2.89 | 1.42 | 5.38 |

convergence process of identified damage extents $\alpha_{15}$, $\alpha_{33}$, $\alpha_{42}$ by the proposed QHEA without measurement noise. Around 366 iterations are needed for QHEA when the termination condition is satisfied. The identified damage extents are $\alpha_{15} = 0.2967$, $\alpha_{33} = 0.2003$,$\alpha_{42} = 0.1475$, and they can gradually converge to the predefined damage severities after approximate 300 iterations.

#### 4.3.2. *Comparison with other algorithms*

In this section, for the comparison purpose, four different heuristic algorithms, including modified differential evolution algorithm (MDE)

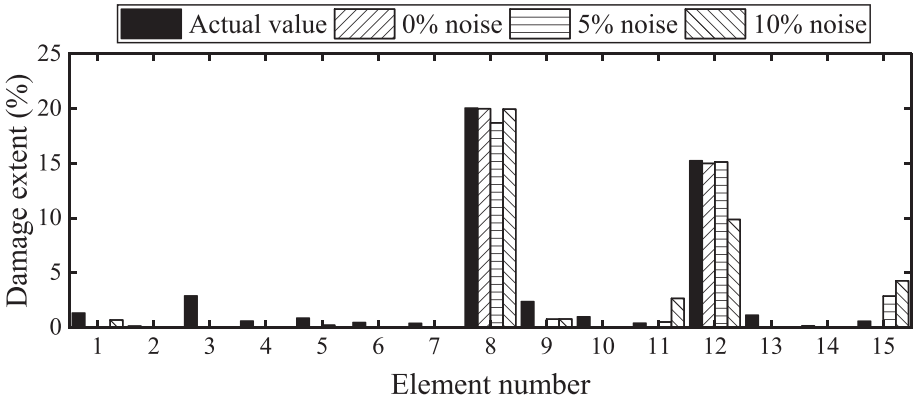


**Fig. 10.** Identified damage extent with modeling error.

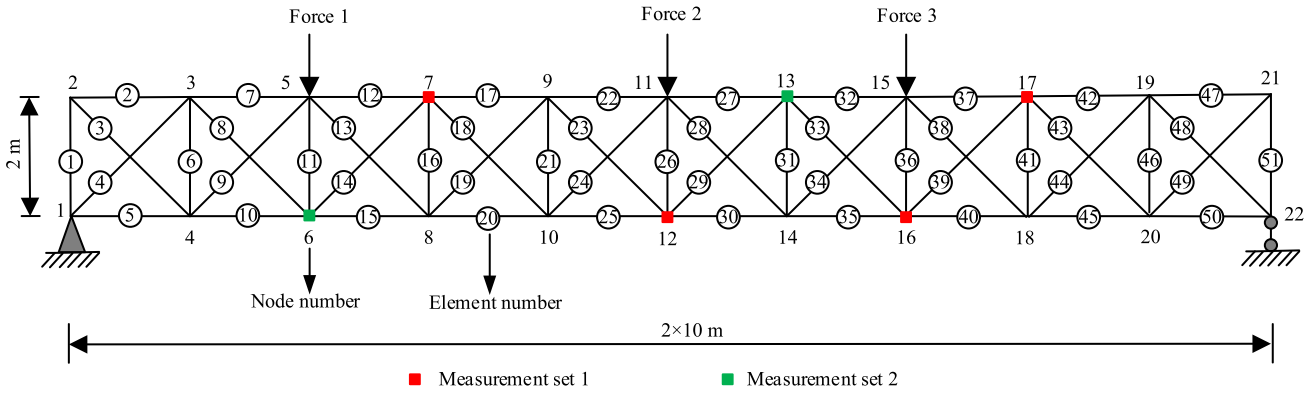


**Fig. 11.** The finite element model of 51-bar truss structure.

[59], Jaya algorithm, improved Jaya algorithm (I-Jaya) [48] and the proposed QHEA are used to estimate structural damages. QHEA is developed by integrating Jaya algorithm, differential evolution, Q-learning algorithm. MDE, Jaya, I-Jaya are used for further comparison with QHEA because these three algorithms are more or less related to the proposed QHEA. Therefore, the improved performance of the proposed QHEA could be better demonstrated by comparing these three relevant algorithms. The parameter settings of MDE, Jaya, I-Jaya, QHEA are listed in Table 5. To ensure the effectiveness, the average values of five independent runs are taken as the final results. Another damage case is assumed that there are 30 %, 15 %, 30 % and 15 % reductions of stiffness at the 10th, 21th, 38th, 45th elements in truss structure, that is, $\alpha_{10} = 0.3, \alpha_{21} = 0.15, \alpha_{38} = 0.3, \alpha_{45} = 0.15$.

Regarding the results, the statistical results from 30 independent runs [60] are used. Fig. 15 depicts the evolutionary process of objective function based on four optimization algorithms. The calculated objective function values of MDE, Jaya, I-Jaya, QHEA are 0.0201, 0.0337, 0.0074 and 9.76E-4, respectively. Obviously, the proposed algorithm is able to achieve more favorable convergence speed owing to the successful combination of Jaya algorithm, DE, and Q-learning algorithm. Only 332 iterations are required to reach convergence tolerance, which demonstrates the superiority of QHEA. The final identification results of damage extents with MDE, Jaya, I-Jaya, QHEA are presented in Fig. 16 and Table 6, respectively. It is noted that several false identifications obtained by MDE are observed at elements 18, 20, 36, 41, and four damaged elements cannot be accurately detected. Likewise, Jaya algorithm fails in identifying damage locations and extents accurately with a poor result of maximum error up to 14.78 %. Compared with MDE and Jaya, less false identifications are noticed from I-Jaya algorithm, but it fails to estimate the damage extents at element 38. In contrast, as illustrated in Fig. 16, the most satisfactory performance is achieved by QHEA with 1.63 % maximum error and 0.21 % mean error.

Herein, the underlying reason of how QHEA enhances the identification results is provided. Fig. 17 presents the selection proportion for the four strategies in QHEA with iterations. It is observed the proportions fluctuate intensively, especially in the initial 80 iterations. After 200 iterations, the selection proportions still have some fluctuations due to the essence of the random searching of the heuristic algorithm. The DE/rand/1 and DE/rand/2 have more selection proportions than DE/current-to-best/1 and Jaya mutation. Different from the relatively single and monotonous search mode in MDE, Jaya and I-Jaya, the proposed QHEA can enable individuals adaptively and continuously select the most suitable search operation from four different search mode in strategy pool under the guidance of the Q-learning so that the balance between global exploration and local exploitation of QHEA is better realized, which indicates the necessity of introducing the Q-learning into evolutionary algorithm. The convergence is accelerated owing to integrating the advantages of Jaya, DE and Q-learning algorithm.

As illustrated in Ref. [61], the robustness is measured by how little variance there is in the identified results reported by each algorithm among their adequate runs. Therefore, the robustness comparisons of the algorithms can be conducted by checking the standard deviations [62]. The high inconsistency between its results indicates that it is not robust. In Section 4.1 CEC2005 benchmark tests, the proposed QHEA is compared with ESAO, IGHS, MPSO, SAMSO. The statistical results from 30 independent runs for the 30 and 50-dimensional tests are used. Obviously, by Table 1 and Table 2, the standard deviations calculated by the proposed QHEA are smaller than ESAO, IGHS, MPSO, SAMSO, which implies the superior robustness of QHEA. Similarly, it can be observed from Table 6 that smaller standard deviations are achieved by QHEA. Thus, the proposed QHEA is a more robust algorithm compared to MDE, Jaya, I-Jaya.

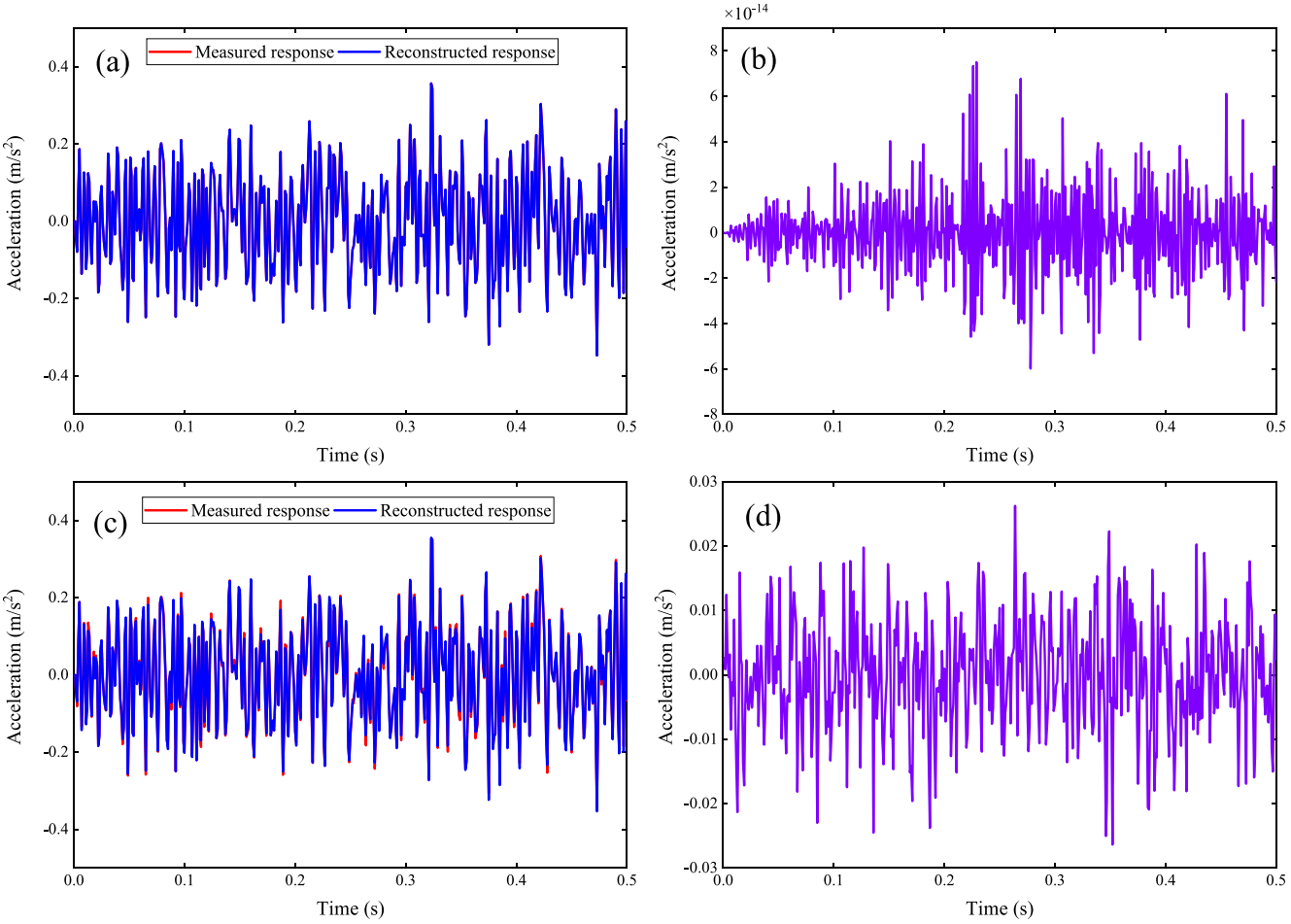


**Fig. 12.** Measured and reconstructed responses of node 13: (a) comparison without noise; (b) error without noise; (c) comparison with 5% noise; (d) error with 5% noise.

## 5. Experimental studies

### 5.1. Introduction of frame model

Experimental tests on a five-floor steel frame model in the laboratory [10] are carried out to further validate the applicability of the proposed method. The process of experimental operation and experimental setup are shown in Fig. 18 and Fig. 19, respectively. The specified waveform signal generated by the computer is input the power amplifier. Then, the expected force is output by a vibration exciter (Modal Shop 2100E11) to excite the frame structure. External excitation is applied to the top floor. The horizontal acceleration responses of each floor are measured by five model 991C accelerometers with the Quantum X data acquisition system. The model 991C accelerometer (V09001) produced by the Institute of Engineering Mechanics of China Earthquake Administration has good impact resistance, and its main specifications are: sensitivity 0.3 $V{\cdot}s^2/m$, measurement range $\pm$ 20 $m/s^2$, frequency passband 0.1–100 Hz, resolution 5 $\times$ $10^{-6}$ $m/s^2$. In terms of geometric dimensions, the height, length, and width of the frame are 1750 mm, 300 mm and 400 mm, respectively. In each floor, there are four identical columns with the cross-section of 40 mm $\times$ 4 mm. The mass density and initial elastic modulus of steel material are approximately 7850 kg/m$^3$ and 206 GPa, respectively. Fig. 20 shows the excitation system and measurement direction of structural responses. A force sensor (PCB-208C02) with a sensitivity of 49.59 mV/lbf is installed to measure the time history of input force. According to the theory of response reconstruction technique, acceleration responses are divided into two measurement sets. The first set includes acceleration measurements of the 1st, 3rd, 5th floors, and the second set contains acceleration measurements of the 2nd and 4th floors. The 20 s vibration data with sampling frequency of 50 Hz is selected for initial model updating and damage identification.

The structure in Fig. 19 can be modeled as a 5-DOFs shear-type lumped mass building [10]. The total masses of each floor including accelerometer can be estimated based on the geometric information and material property: $M_1 = 24.99$ kg, $M_2 = 24.94$ kg, $M_3 = 24.93$ kg, $M_4 = 24.75$ kg, $M_5 = 24.80$ kg. The story stiffness is composed by the lateral stiffness of four columns. Thus, the theoretical story stiffness can be calculated as

$$K_i = 4 \times \frac{12EI}{l^3}, i = 1, 2, 3, 4, 5 \tag{35}$$

where $E$ is the elastic modulus; $I$ is moment of inertia, $I = \frac{bh^3}{12}$.

It is noted that the simplified initial FE model has discrepancy with the physical model. Thus, the initial finite element model needs to be calibrated. Model updating under intact state is implemented by adjusting the structural stiffness parameters with QHEA. The measured accelerations from the 2nd, 4th floors and reconstructed ones are set as objective function. Population size and maximum iterations of QHEA are taken as 40 and 100, and search space limits are [0.8, 1.2]. It is noticed from Fig. 21 the stiffness parameters of five story stiffness are updated with iterations. The final updated stiffness parameters are $\theta_1 = 0.978$, $\theta_2 = 1.036$,$\theta_3 = 1.054$, $\theta_4 = 0.937$, $\theta_5 = 1.024$, and story stiffness for each floor is different owing to the deviations of dimension, properties of materials, boundary conditions, etc. By Fig. 22, the calculated responses

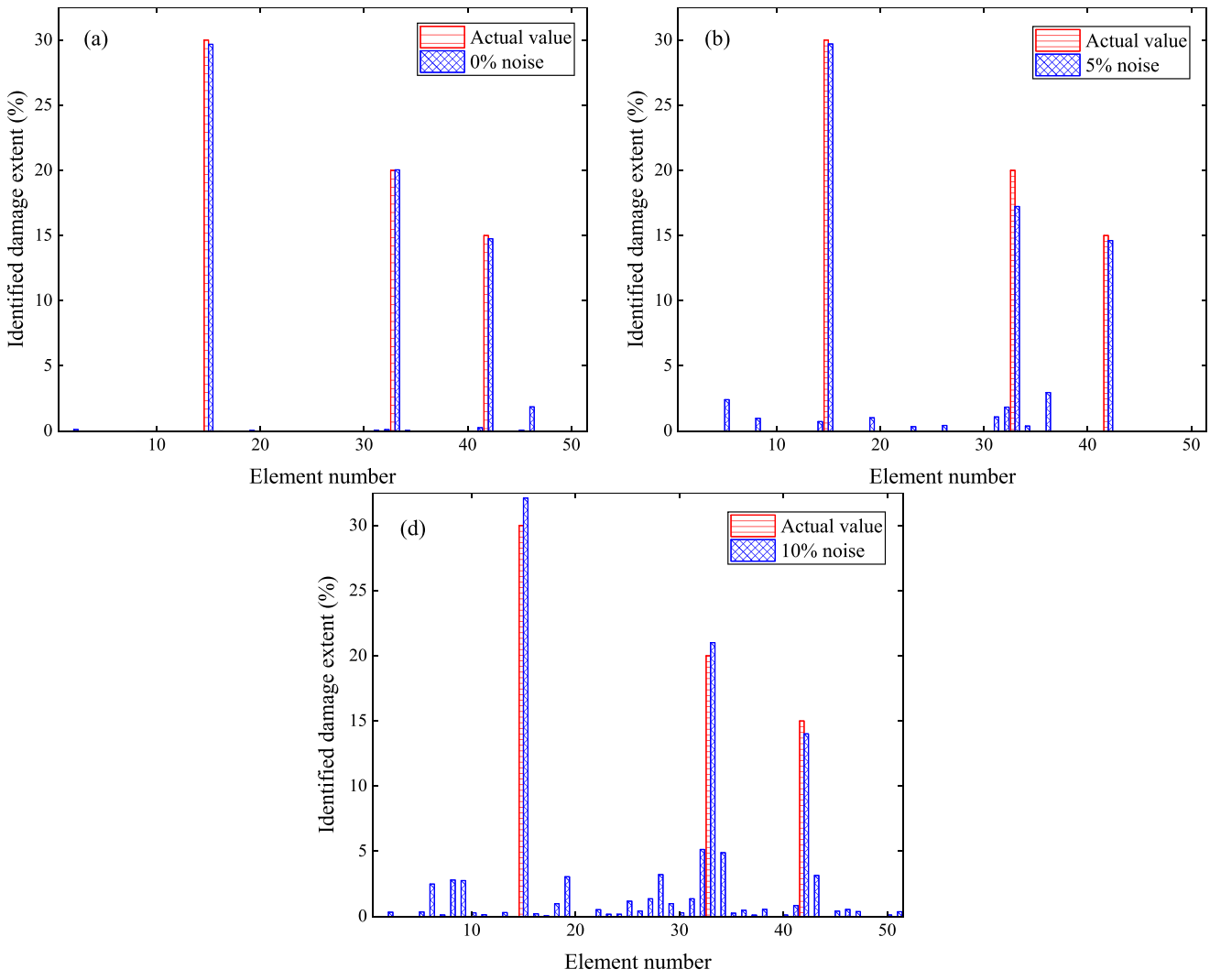


**Fig. 13.** Identified damage extents using QHEA with: (a) 0% noise; (b) 5% noise; (c) 10% noise.

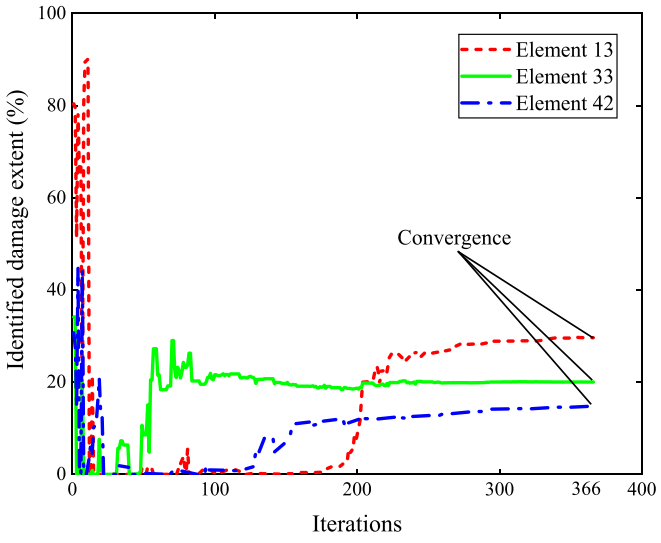


**Fig. 14.** Convergence process of the damage elements by the proposed QHEA (noise free).

**Table 5**
The parameter settings of MDE, Jaya, I-Jaya, QHEA.

| Parameters | MDE[59] | Jaya | I-Jaya[48] | QHEA |
|---|---|---|---|---|
| Population size *NP* | 100 | 100 | 100 | 100 |
| Maximum iterations *Max_Iter* | 400 | 400 | 400 | 400 |
| Tolerance *Tol* | $5\times10^{-3}$ | $5\times10^{-3}$ | $5\times10^{-3}$ | $5\times10^{-3}$ |
| Mutation rate | 0.4 | | | 0.8 |
| Crossover rate | [0-1] | | | 0.9 |
| Threshold value | 0.1 | | | |
| Discount factor | | | | 0.8 |
| Total evaluations | 40000 | 40000 | 40000 | 40000 |

from the numerical model could agree well with the measured ones. The relative errors are 4.97 % and 3.95 % for the second floor and the fourth floor, respectively. Therefore, the updated finite element model can simulate the responses of experimental model after model updating. The updated structural parameters could be regarded as baseline for subsequent damage detection.

### 5.2. *Identification results with the proposed method*

The acceleration responses of the measurement set 2 can be reconstructed using the responses of measurement set 1 and response reconstruction technique. Structural damages are identified by optimizing the

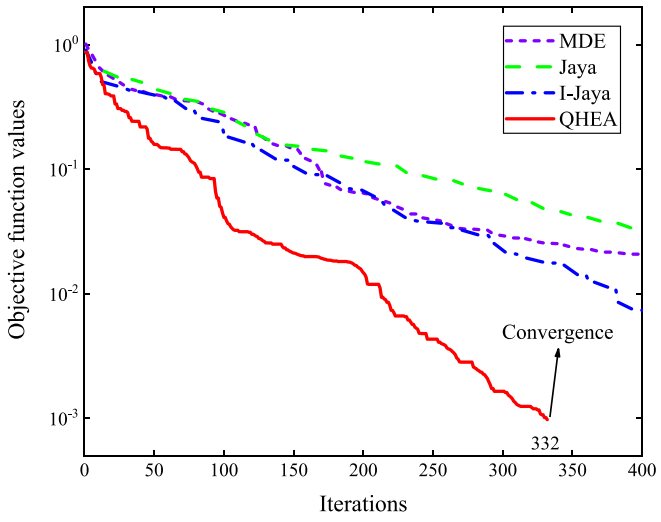


**Fig. 15.** The evolutionary process of objective function based on four algorithms.

objective function defined based on the measured accelerations and reconstructed ones in the measurement set 2. Only QHEA is utilized as search tool considering its more superior performance than MDE, Jaya, I-Jaya. The parameter settings of QHEA are defined as the same values in the Table 5. According to the Eq. (35), the damage can be introduced by reducing the width of column. Two damage cases are studied. In case 1, 10 % equivalent stiffness reduction is introduced in the fifth floor by replacing original four columns to thinner ones. In case 2, 20 % equivalent stiffness reduction is introduced in the fourth floor in the same way. Herein, mass alteration could be neglected because there are only less than 2 % slight reductions of mass in these two damage cases.

In each damage case, four tests are implemented and their mean values are considered as the identified damage results. Fig. 23(a) and

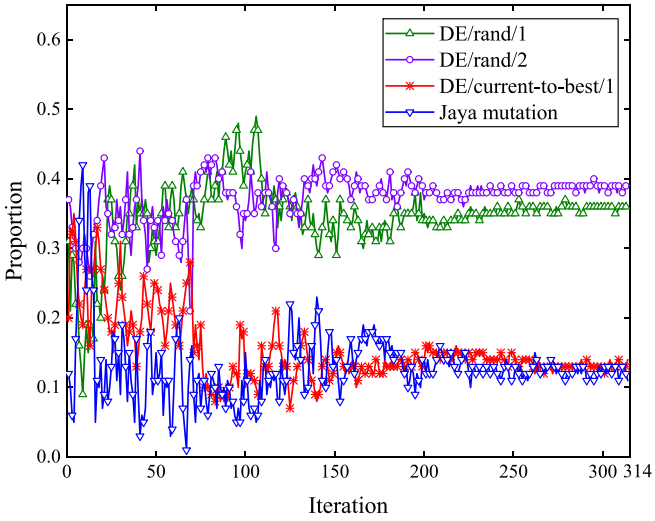


**Fig. 17.** Search proportion for the four strategies in the proposed QHEA.

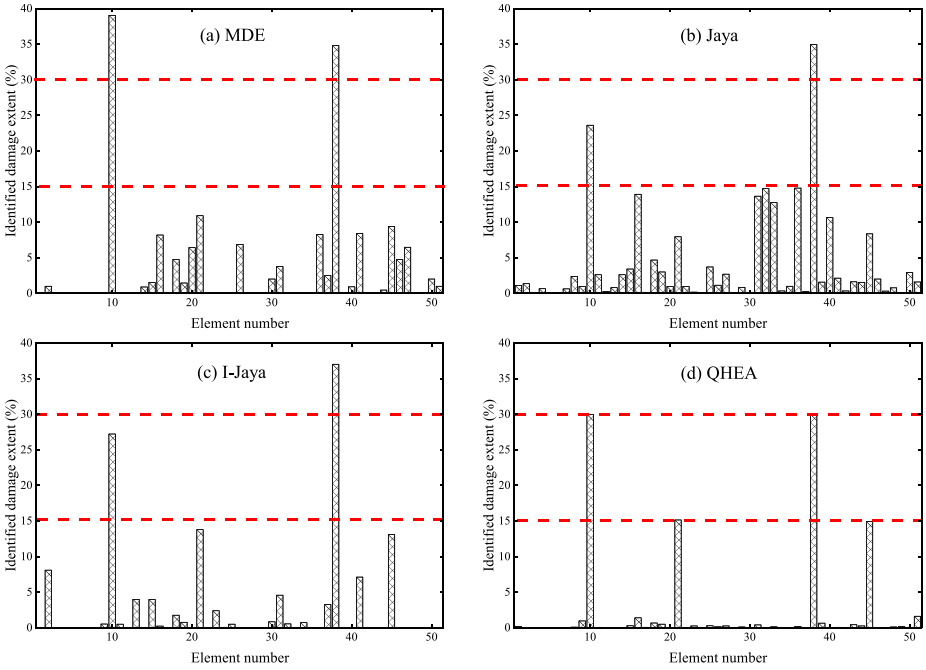


**Fig. 16.** Identification results with MDE, Jaya, I-Jaya, QHEA.

**Table 6**
Identified damage extents of truss structure with four different algorithms.

| Damage location | True value | MDE | | Jaya | | I-Jaya | | QHEA | |
|---|---|---|---|---|---|---|---|---|---|
| | | Mean | Std. | Mean | Std. | Mean | Std. | Mean | Std. |
| $\alpha_{10}$ | 0.30 | 0.3905 | 0.066 | 0.2362 | 0.035 | 0.2724 | 0.010 | 0.2999 | 1.05E-04 |
| $\alpha_{21}$ | 0.15 | 0.1090 | 0.052 | 0.079 | 0.024 | 0.1378 | 0.012 | 0.1514 | 8.16 E-04 |
| $\alpha_{38}$ | 0.30 | 0.3482 | 0.048 | 0.3495 | 0.008 | 0.3703 | 0.028 | 0.30 | 4.02E-05 |
| $\alpha_{45}$ | 0.15 | 0.0940 | 0.030 | 0.084 | 0.041 | 0.1310 | 0.019 | 0.1493 | 2.17E-04 |

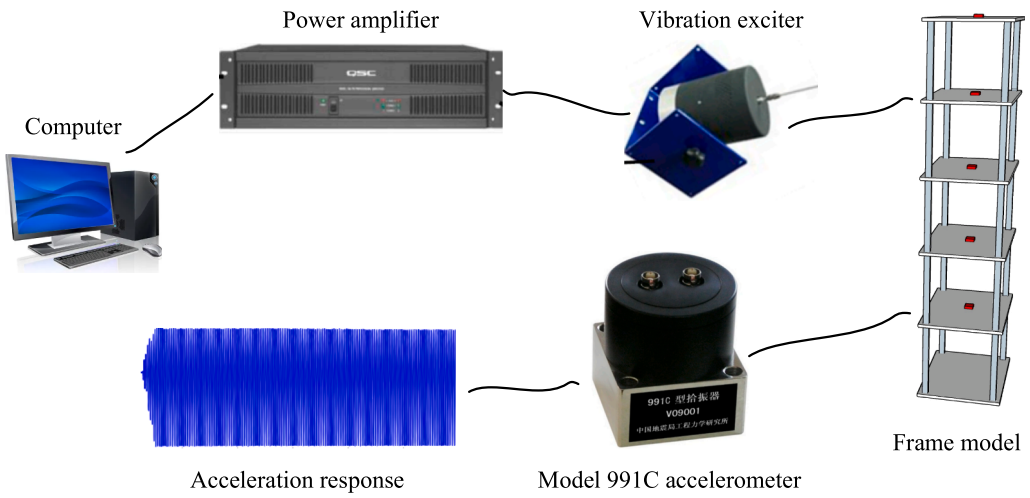


**Fig. 18.** The process of experimental operation.

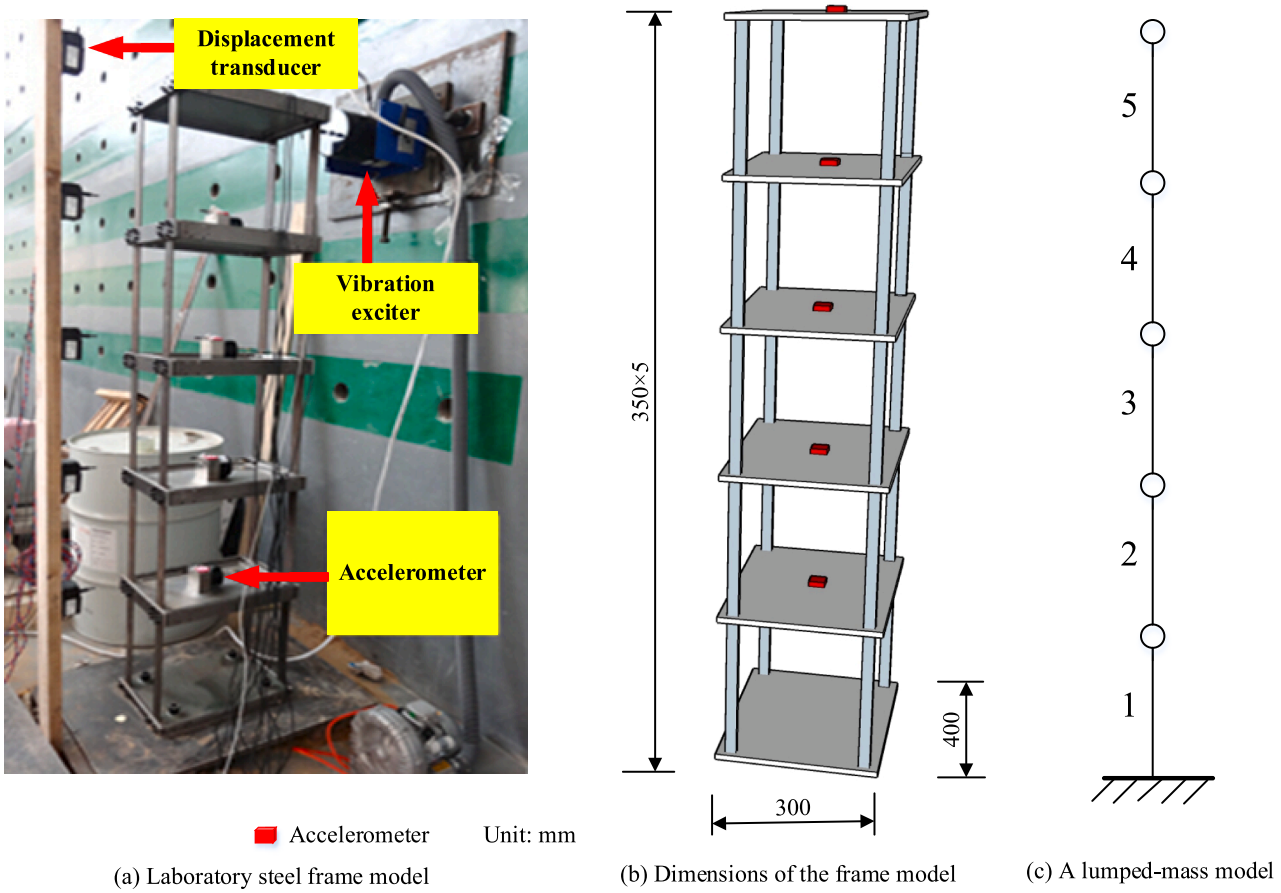


**Fig. 19.** Five-story steel frame structure in the laboratory.

Fig. 23(b) present the identification results for damage case 1 and case 2, respectively. Obviously, damage locations and extents are successfully detected. More specifically, in damage case 1, damage extent at the 5th floor is identified as 12.19 %, which is sufficient accuracy with the actual value. In damage case 2, damage extent at the 4th floor is identified as 21.68 %. Some false identifications are noticed with maximum values 2.88 % at element 1 for case 1 and 2.89 % at element 3 for case 2. These minor errors may be caused by measurement noise and environmental conditions. The average results obtained by multiple tests demonstrate that the proposed identification approach is able to accurately and effectively detect, localize, and quantify structural damages with output-only experimental data.

## 6. Conclusions

In the present paper, a novel output-only detection identification approach based on QHEA and response reconstruction technique is proposed. The unknown input excitation and structural dynamic

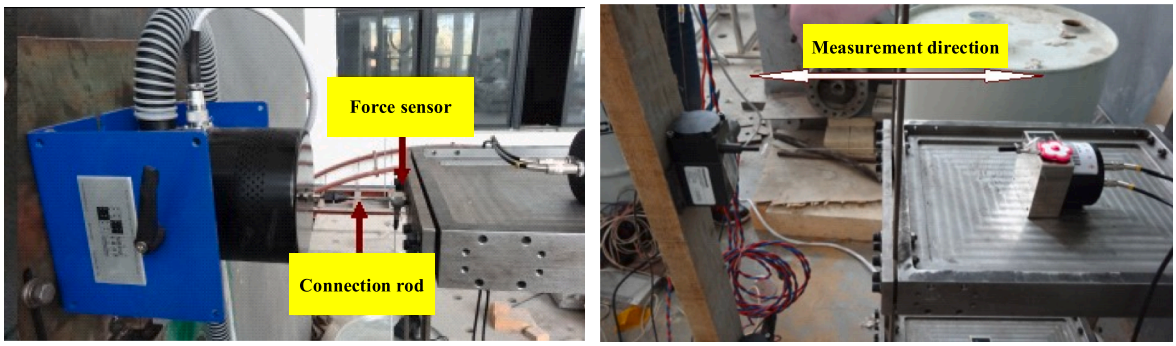


(a) Exert input excitation (b) Measurement direction

**Fig. 20.** The excitation system and measurement direction of structural responses.

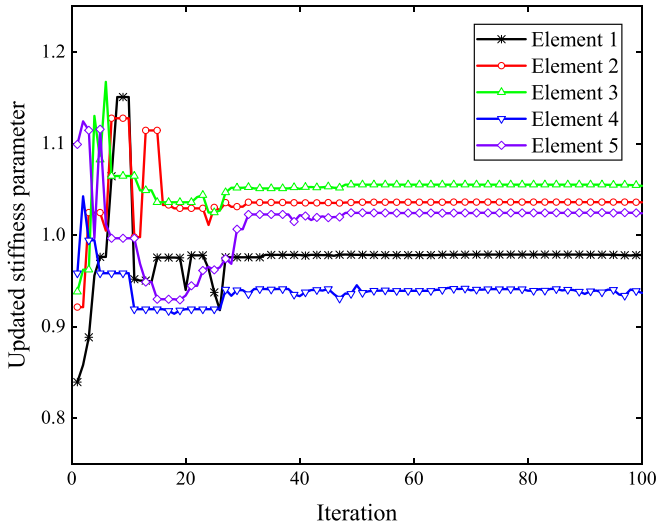


**Fig. 21.** The updated stiffness parameters with iterations.

responses can be reconstructed using unit impulse response function and Duhamel's integral in time domain. The difference between the measured accelerations belonging to measurement set 2 and reconstructed ones is defined as objective function. To deal with the optimization-based structural damage identification problem, a new framework QHEA integrating Jaya algorithm, DE and Q-learning algorithm is developed. The CEC2005 benchmark functions are optimized by the proposed QHEA and its superiority is validated by comparing with ESAO, IGHS, MPSO, SAMSO. Numerical studies on a cantilever beam structure under single excitation and a simply-supported truss structure under multiple input forces are implemented to validate the effectiveness and superiority of the proposed method. Furthermore, laboratory tests on a five-floor steel frame structure are conducted. Some conclusions can be summarized from numerical and experimental studies as follows:

(1) Compared with MDE, Jaya, I-Jaya, the proposed QHEA can achieve more favorable results with 1.63 % maximum error and 0.21 % mean error. owing to the adaptive selection of the best search strategy from the strategy pool in each iteration under the guidance of Q-learning, which indicates the balance between exploration and exploitation of QHEA is well realized.
(2) The unknown input force and output acceleration responses can be accurately reconstructed with response reconstruction and Tikhonov regularization technique with limited noise-polluted measurement data. For example, the relative error and Pearson correlation coefficient are 10.46 % and 0.9942, respectively, for the reconstructed acceleration response at node 4, which is significant to accurately acquire the dynamic responses of civil structures at locations where no sensors installed.
(3) Taking both the measurement noise and modeling errors into consideration, the presented damage identification method can still provide successful damage detection results, showing its robustness in structural damage identification. Only 5.38 %

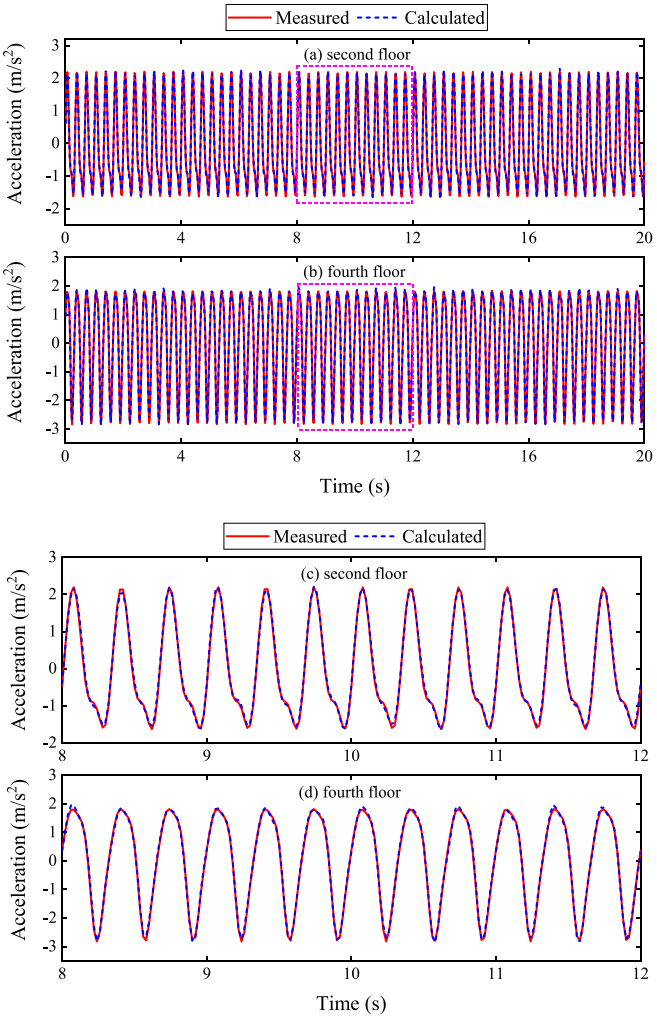


**Fig. 22.** Measured and calculated acceleration responses after updating: (a) second floor (0–20 s); (b) fourth floor (0–20 s); (c) second floor (8–12 s); (b) fourth floor (8–12 s).

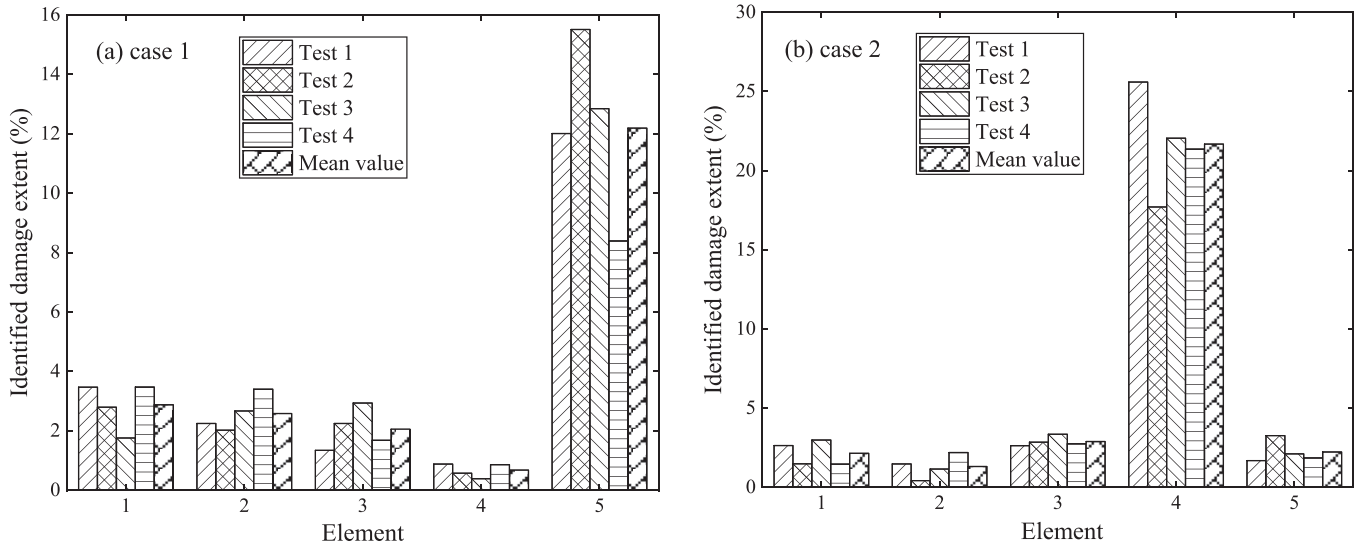


**Fig. 23.** Identified damage results with proposed output-only method: (a) case 1; (b) case 2.

maximum identification error and 1.42 % mean error are obtained considering modeling error and 10 % measurement noise.

(4) In all studies considered, the presented output-only approach based on QHEA and response reconstruction technique is able to accurately detect damage locations and extents without the measurement of input force.

However, the present work has some limitations. The time histories of the unknown input forces are not required but the locations of these external excitations should be assumed known. In fact, the force location is difficult to be determined for structure under ambient excitation or traffic loads, which limits the practical application to some extent. Besides, the proposed method requires the number of sensors in the measurement set 1 exceeds the number of unknown external excitations on the structure, which is difficult to meet under some conditions. Finally, only single type of structural response is utilized in the present paper. From the practical point of view, a large civil structure is usually equipped with a multi-sensor monitoring system. Thus, various types of structural responses, such as acceleration, strain, displacement, are available for damage identification. The authors are conducting the investigation of structural damage identification with output-only heterogeneous data fusion.

## CRediT authorship contribution statement

**Guangcai Zhang:** Investigation, Methodology, Software, Writing – original draft. **Jianfei Kang:** Visualization, Investigation. **Chunfeng Wan:** Supervision, Conceptualization. **Liyu Xie:** Writing – review & editing. **Songtao Xue:** Funding acquisition, Conceptualization and reviewing.

## Declaration of competing interest

The authors declare that they have no known competing financial interests or personal relationships that could have appeared to influence the work reported in this paper.

## Data availability

Data will be made available on request.

## Acknowledgments

This work was supported by the National Key R&D Program of China (2021YFE0112200), the Japan Society for Promotion of Science (Kakenhi No. 18K04438), the Tohoku Institute of Technology research Grant and the Postgraduate Research&Practice Innovation Program of Jiangsu Province (KYCX23_0273). These financial supports are sincerely appreciated. Besides, the author would like to thank the anonymous reviewers for their detailed and fruitful remarks.

## References

[1] Y.H. An, E. Chatzi, S.H. Sim, et al., Recent progress and future trends on damage identification methods for bridge structures, Struct Control Health Monit 26 (10) (2019) e2416.
[2] R.R. Hou, Y. Xia, Review on the new development of vibration-based damage identification for civil engineering structures: 2010–2019, J Sound and Vib 491 (2021), 115741, https://doi.org/10.1016/j.jsv.2020.115741.
[3] P. Kot, M. Muradov, M. Gkantou, et al., Recent advancements in non-destructive testing techniques for structural health monitoring, Appl Sci 11 (6) (2021) 2750, https://doi.org/10.3390/app11062750.
[4] S. Umar, N. Bakhary, A.R.Z. Abidin, Response surface methodology for damage detection using frequency and mode shape, Measurement 115 (2018) 258–268, https://doi.org/10.1016/j.measurement.2017.10.047.
[5] Q.Y. Ma, M. Solís, J.D. Rodríguez-Mariscal, et al., Wavelet and Lipschitz exponent based damage identification method for beams using mode shapes, Measurement 205 (2022), 112201, https://doi.org/10.1016/j.measurement.2022.112201.
[6] K. Liu, R.J. Yan, C.G. Soares, Damage identification in offshore jacket structures based on modal flexibility, Ocean Eng 170 (2018) 171–185, https://doi.org/10.1016/j.oceaneng.2018.10.014.
[7] A. Kaveh, A. Zolghadr, Cyclical parthenogenesis algorithm for guided modal strain energy based structural damage detection, Appl Soft Comput 57 (2017) 250–264, https://doi.org/10.1016/j.asoc.2017.04.010.
[8] S.M.H. Pooya, A. Massumi, A novel and efficient method for damage detection in beam-like structures solely based on damaged structure data and using mode shape curvature estimation, Appl Math Model 91 (2021) 670–694, https://doi.org/10.1016/j.apm.2020.09.012.
[9] J.N. Yang, S. Lin, Identification of parametric variations of structures based on least squares estimation and adaptive tracking technique, J Eng Mech 131 (3) (2005) 290–298, https://doi.org/10.1061/(ASCE)0733-9399(2005)131:3(290).
[10] L.Y. Xie, Z.W. Zhou, L. Zhao, et al., Parameter identification for structural health monitoring with extended Kalman filter considering integration and noise effect, Appl Sci 8 (12) (2018) 2480, https://doi.org/10.3390/app8122480.
[11] Xue ST, Wen B, Huang R, et al. Parameter identification for structural health monitoring based on Monte Carlo method and likelihood estimate. Int J Distrib Sens N 2018;14(7):1550147718786888. https://doi.org/10.1177/1550147718786888.
[12] Z.R. Lu, L. Wang, An enhanced response sensitivity approach for structural damage identification: convergence and performance, Int J Numer Methods Eng 111 (13) (2017) 1231–1251, https://doi.org/10.1002/nme.5502.
[13] E.N. Chatzi, A.W. Smyth, Particle filter scheme with mutation for the estimation of time-invariant parameters in structural health monitoring applications, Struct

Control Health Monit 20 (7) (2013) 1081–1095, https://doi.org/10.1002/stc.1520.
[14] J. Chen, J. Li, Simultaneous identification of structural parameters and input time history from output-only measurements, Comput Mech 33 (5) (2004) 365–374, https://doi.org/10.1007/s00466-003-0538-9.
[15] Z.R. Lu, S.S. Law, Identification of system parameters and input force from output only, Mech Syst Signal Process 21 (5) (2007) 2099–2111, https://doi.org/10.1016/j.ymssp.2006.11.004.
[16] Q. Zhang, Ł. Jankowski, Z. Duan, Simultaneous identification of excitation time histories and parametrized structural damages, Mech Syst Signal Process 33 (2012) 56–68, https://doi.org/10.1016/j.ymssp.2012.06.018.
[17] H. Sun, R. Betti, Simultaneous identification of structural parameters and dynamic input with incomplete output-only measurements, Struct Control Health Monit 21 (6) (2014) 868–889, https://doi.org/10.1002/stc.1619.
[18] V. Jayalakshmi, A. Rao, Simultaneous identification of damage and input dynamic force on the structure for structural health monitoring, Struct Multidisc Optim 55 (6) (2017) 2211–2238, https://doi.org/10.1007/s00158-016-1637-5.
[19] P.H. Ni, Y. Xia, J. Li, et al., Improved decentralized structural identification with output-only measurements, Measurement 122 (2018) 597–610, https://doi.org/10.1016/j.measurement.2017.09.029.
[20] Ni PH, Xia Yong, Law SS, et al. Structural damage detection using auto/cross-correlation functions under multiple unknown excitations. Int J Struct Stab Dyn 2014;14(05):1440006. https://doi.org/10.1142/S0219455414400069.
[21] X.J. Wang, G.C. Zhang, X.M. Wang, et al., Output-only structural parameter identification with evolutionary algorithms and correlation functions, Smart Mater Struct 29 (3) (2020), 035018, https://doi.org/10.1088/1361-665X/ab6ce9.
[22] X.Y. Li, L.X. Wang, S.S. Law, Damage Detection for Structures under Ambient Vibration via Covariance of Covariance Matrix and Consistent Regularization, Adv Struct Eng 16 (1) (2013) 77–86, https://doi.org/10.1260/1369-4332.16.1.77.
[23] Y. Lei, D.D. Xia, F. Chen, et al., Synthesis of cross-correlation functions of partial responses and the extended Kalman filter approach for structural damage detection under ambient excitations, Int J Struct Stab Dyn 18 (08) (2018) 1840003, https://doi.org/10.1142/S0219455418400035.
[24] G.C. Zhang, C.F. Wan, X.B. Xiong, et al., Output-only structural damage identification using hybrid Jaya and differential evolution algorithm with reference-free correlation functions, Measurement 199 (2022), 111591, https://doi.org/10.1016/j.measurement.2022.111591.
[25] X.J. Wang, F. Chen, H.Y. Zhou, et al., Structural damage detection based on cross-correlation function with data fusion of various dynamic measurements, J Sound Vib 541 (2022), 117373, https://doi.org/10.1016/j.jsv.2022.117373.
[26] J.J. He, X.F. Guan, Y.M. Liu, Structural response reconstruction based on empirical mode decomposition in time domain[J], Mech Syst Signal Process 28 (2012) 348–366, https://doi.org/10.1016/j.ymssp.2011.12.010.
[27] C.D. Zhang, Y.L. Xu, Structural damage identification via multi-type sensors and response reconstruction, Struct Health Monit 15 (6) (2016) 715–729, https://doi.org/10.1177/1475921716659787.
[28] Y.H. Hong, H.K. Kim, H.S. Lee, Reconstruction of dynamic displacement and velocity from measured accelerations using the variational statement of an inverse problem, J Sound Vib 329 (23) (2010) 4980–5003, https://doi.org/10.1016/j.jsv.2010.05.016.
[29] S.S. Law, J. Li, Y. Ding, Structural response reconstruction with transmissibility concept in frequency domain, Mech Syst Signal Process 25 (3) (2011) 952–968, https://doi.org/10.1016/j.ymssp.2010.10.001.
[30] W.J. Yan, M.Y. Zhao, Q. Sun, et al., Transmissibility-based system identification for structural health Monitoring: Fundamentals, approaches, and applications, Mech Syst Signal Process 117 (2019) 453–482, https://doi.org/10.1016/j.ymssp.2018.06.053.
[31] J. Li, S.S. Law, Y. Ding, Substructure damage identification based on response reconstruction in frequency domain and model updating, Eng Struct 41 (2012) 270–284, https://doi.org/10.1016/j.engstruct.2012.03.035.
[32] J. Li, H. Hao, Substructure damage identification based on wavelet-domain response reconstruction, Struct Health Monit 13 (4) (2014) 389–405, https://doi.org/10.1177/1475921714532991.
[33] H.P. Zhu, L. Mao, S. Weng, A sensitivity-based structural damage identification method with unknown input excitation using transmissibility concept, J Sound Vib 333 (26) (2014) 7135–7150, https://doi.org/10.1016/j.jsv.2014.08.022.
[34] P.H. Ni, Q. Han, X.L. Du, et al., Bayesian model updating of civil structures with likelihood-free inference approach and response reconstruction technique, Mech Syst Signal Process 164 (2022), 108204, https://doi.org/10.1016/j.ymssp.2021.108204.
[35] Z.P. Chen, L. Yu, A new structural damage detection strategy of hybrid PSO with Monte Carlo simulations and experimental verifications, Measurement 122 (2018) 658–669, https://doi.org/10.1016/j.measurement.2018.01.068.
[36] M.S. Huang, X.H. Cheng, Y.Z. Lei, Structural damage identification based on substructure method and improved whale optimization algorithm, J Civ Struct Health 11 (2021) 351–380, https://doi.org/10.1007/s13349-020-00456-7.
[37] Z.H. Ding, K.S. Fu, W. Deng, et al., A modified Artificial Bee Colony algorithm for structural damage identification under varying temperature based on a novel objective function, Appl Math Model 88 (2020) 122–141, https://doi.org/10.1016/j.apm.2020.06.039.
[38] H.Y. Zhou, G.C. Zhang, X.J. Wang, et al., Structural identification using improved butterfly optimization algorithm with adaptive sampling test and search space reduction method, Structures 33 (2021) 2121–2139, https://doi.org/10.1016/j.istruc.2021.05.043.
[39] R. Ghiasi, H. Fathnejat, P. Torkzadeh, A three-stage damage detection method for large-scale space structures using forward substructuring approach and enhanced bat optimization algorithm, Eng Comput 35 (3) (2019) 857–874, https://doi.org/10.1007/s00366-018-0636-0.
[40] S.C. Xie, H.C. Tan, Y.X. Li, et al., Locally generalized preserving projection and flexible grey wolf optimizer-based ELM for fault diagnosis of rolling bearing, Measurement 202 (2022), 111828, https://doi.org/10.1016/j.measurement.2022.111828.
[41] S. Das, P. Saha, Performance of swarm intelligence based chaotic meta-heuristic algorithms in civil structural health monitoring, Measurement 169 (2021), 108533, https://doi.org/10.1016/j.measurement.2020.108533.
[42] W. Hare, J. Nutini, S. Tesfamariam, A survey of non-gradient optimization methods in structural engineering, Adv Eng Softw 59 (2013) 19–28, https://doi.org/10.1016/j.advengsoft.2013.03.001.
[43] N.I. Kim, S. Kim, J. Lee, Vibration-based damage detection of planar and space trusses using differential evolution algorithm, Appl Acoust 148 (2019) 308–321, https://doi.org/10.1016/j.apacoust.2018.08.032.
[44] Z.H. Ding, J. Li, H. Hao, et al., Nonlinear hysteretic parameter identification using an improved tree-seed algorithm, Swarm Evol Comput 46 (2019) 69–83, https://doi.org/10.1016/j.swevo.2019.02.005.
[45] R. Rao, Jaya: A simple and new optimization algorithm for solving constrained and unconstrained optimization problems, Int J Ind Eng Comp 7 (1) (2016) 19–34, https://doi.org/10.5267/j.ijiec.2015.8.004.
[46] A. Kaveh, S.M. Hosseini, A. Zaerreza, Improved Shuffled Jaya algorithm for sizing optimization of skeletal structures with discrete variables, Structures 29 (2021) 107–128, https://doi.org/10.1016/j.istruc.2020.11.008.
[47] K.J. Yu, B.Y. Qu, C.T. Yue, et al., A performance-guided JAYA algorithm for parameters identification of photovoltaic cell and module, Appl Energ 237 (2019) 241–257, https://doi.org/10.1016/j.apenergy.2019.01.008.
[48] Z.H. Ding, J. Li, H. Hao, Structural damage identification using improved Jaya algorithm based on sparse regularization and Bayesian inference, Mech Syst Signal Process 132 (2019) 211–231, https://doi.org/10.1016/j.ymssp.2019.06.029.
[49] G.C. Zhang, J.L. Hou, C.F. Wan, et al., Structural system identification and damage detection using adaptive hybrid Jaya and differential evolution algorithm with mutation pool strategy, Structures 46 (2022) 1313–1326, https://doi.org/10.1016/j.istruc.2022.10.130.
[50] R. Gämperle, S.D. Müller, P. Koumoutsakos, A parameter study for differential evolution, Int J Fuzzy Log Intell Syst 10 (10) (2002) 293–298.
[51] Y.H. Wang, T.H.S. Li, C.J. Lin, Backward Q-learning: The combination of Sarsa algorithm and Q-learning, Eng Appl Artif Intell 26 (9) (2013) 2184–2193, https://doi.org/10.1016/j.engappai.2013.06.016.
[52] Kaveh A, Dadras Eslamlou A, Rahmani P, et al. Optimal sensor placement in large-scale dome trusses via Q-learning-based water strider algorithm. Struct Control Health Monit 2022:e2949. https://doi.org/10.1002/stc.2949.
[53] Z.H. Ding, L.F. Li, X.Y. Wang, et al., Vibration-based FRP debonding detection using a Q-learning evolutionary algorithm, Eng Struct 275 (2023), 115254, https://doi.org/10.1016/j.engstruct.2022.115254.
[54] X. Wang, G.G. Wang, B. Song, et al., A novel evolutionary sampling assisted optimization method for high-dimensional expensive problems, IEEE Trans Evol Comput 23 (2019) 815–827, https://doi.org/10.1109/TEVC.2019.2890818.
[55] M. El-Abd, An improved global-best harmony search algorithm, Appl Math Comput 222 (2013) 94–106, https://doi.org/10.1016/j.amc.2013.07.020.
[56] H. Liu, X.W. Zhang, L.P. Tu, A modified particle swarm optimization using adaptive strategy, Expert Syst Appl 152 (2020), 113353, https://doi.org/10.1016/j.eswa.2020.113353.
[57] F. Li, X.W. Cai, L. Gao, et al., A surrogate-assisted multiswarm optimization algorithm for high-dimensional computationally expensive problems, IEEE Trans Cybern 51 (3) (2020) 1390–1402, https://doi.org/10.1109/TCYB.2020.2967553.
[58] C.S.N. Pathirage, J. Li, L. Li, et al., Structural damage identification based on autoencoder neural networks and deep learning, Eng Struct 172 (2018) 13–28, https://doi.org/10.1016/j.engstruct.2018.05.109.
[59] D. Dinh-Cong, T. Vo-Duy, V. Ho-Huu, et al., An efficient multi-stage optimization approach for damage detection in plate structures, Adv Eng Softw 112 (2017) 76–87, https://doi.org/10.1016/j.advengsoft.2017.06.015.
[60] Z. Ding, Y. Zhao, Z. Lu, Simultaneous identification of structural stiffness and mass parameters based on Bare-bones Gaussian Tree Seeds Algorithm using time-domain data[J], Applied Soft Computing 83 (2019), 105602, https://doi.org/10.1016/j.asoc.2019.105602.
[61] E. Koessler, A. Almomani, Hybrid particle swarm optimization and pattern search algorithm[J], Optimization and Engineering 22 (2021) 1539–1555, https://doi.org/10.1007/s11081-020-09534-7.
[62] H. Haklı, H. Uğuz, A novel particle swarm optimization algorithm with Levy flight [J], Applied Soft Computing 23 (2014) 333–345, https://doi.org/10.1016/j.asoc.2014.06.034.